

1 **Sea salt reactivity over the northwest Atlantic: An in-depth look**
2 **using the airborne ACTIVATE dataset**

3
4 Eva-Lou Edwards¹, Yonghoon Choi^{2,3}, Ewan C. Crosbie^{2,3}, Joshua P. DiGangi², Glenn S.
5 Diskin², Claire E. Robinson^{2,3,†}, Michael A. Shook², Edward L. Winstead^{2,3}, Luke D. Ziemba²,
6 and Armin Sorooshian^{1,4}

7
8
9 ¹Department of Chemical and Environmental Engineering, University of Arizona, Tucson, AZ,
10 85721, USA

11 ²NASA Langley Research Center, Hampton, VA, 23681, USA

12 ³Analytical Mechanics Associates, Inc., Hampton, VA, 23666, USA

13 ⁴Department of Hydrology and Atmospheric Sciences, University of Arizona, Tucson, AZ,
14 85721, USA

15
16 †Deceased

17
18 *Corresponding author: armin@arizona.edu

19 **Abstract**

20 Chloride (Cl^-) displacement from sea salt particles is an extensively studied phenomenon with
21 implications on human health, visibility, and the global radiation budget. Past works have
22 investigated Cl^- depletion over the northwest Atlantic (NWA), yet an updated, multiseasonal, and
23 geographically expanded account of sea salt reactivity over the region is needed. This study uses
24 chemically resolved mass concentrations and meteorological data from the airborne Aerosol Cloud
25 meTeorology Interactions oVer the western ATlantic Experiment (ACTIVATE) to quantify
26 seasonal, spatial, and meteorological trends in Cl^- depletion and to explore the importance of
27 quantifying (1) non-sea salt sources of Na^+ and (2) mass concentrations of lost Cl^- instead of
28 relative amounts displaced. Lost Cl^- mass concentrations are lowest in December-February and
29 March, moderate around Bermuda in June, and highest in May (median losses of 0.04, 0.04, 0.66,
30 and $1.76 \mu\text{g m}^{-3}$, respectively), with losses in May high enough to potentially accelerate
31 tropospheric oxidation rates. Inorganic acidic species can account for all Cl^- depletion in
32 December-February, March, and June near Bermuda, yet none of the lost Cl^- in May, suggesting
33 organic acids may be of importance for Cl^- displacement in certain months. Contributions of dust
34 to Na^+ are not important seasonally but may cause relevant overestimates of lost Cl^- in smoke and
35 dust plumes. Higher percentages of Cl^- depletion often do not correspond to larger mass
36 concentrations of lost Cl^- , so it is highly recommended to quantify the latter to place depletion
37 reactions in context with their role in atmospheric oxidation and radiative forcing.

1. Introduction

Chlorine (Cl) is a common constituent of trace gases and aerosol particles found in Earth's atmosphere. Chlorine-containing species play a critical role in the global radiation budget for many reasons, including their ability to produce highly reactive Cl radicals. These radicals can perturb atmospheric chemical processes by inducing reactions that would otherwise be less likely to occur and/or accelerating the rates of certain reactions. For example, Cl radicals in the stratosphere can incite reactions that destroy ozone (O₃; Molina and Rowland, 1974; Solomon et al., 2023), therefore allowing increased amounts of shortwave radiation to reach the surface and harmfully affect living beings.

Cl radicals typically react faster with volatile organic compounds (VOCs) compared to hydroxyl radicals (OH; Roberts et al., 2008; Thornton et al., 2010; Young et al., 2014), which has particular importance in the troposphere. Cl radicals oxidize methane ~16 times faster than OH (Faxon and Allen, 2013 and references therein), thus reducing the lifetime of this important greenhouse gas. Accelerated oxidation of methane and other VOCs can result in increased O₃ production near the surface (Knipping and Dabdub, 2003; Pechtl and von Glasow, 2007; Tanaka et al., 2003), which can have deleterious effects on animals (e.g., respiratory problems, increased mortality; Lippmann, 1989; Nuvolone et al., 2018) and plants (e.g., decreased growth and photosynthesis; Wittig et al., 2009). Cl radicals may be responsible for [0.8% of the global oxidation of methane, 14% of ethane, 8% for propane, and 7% for longer-chain alkanes](#) (Wang et al., 2021) ~~[15–27% of VOC oxidation in the global troposphere \(Sherwen et al., 2016\)](#)~~ and can play an exceptionally critical role in governing atmospheric composition in the early morning when OH radicals are less abundant (Young et al., 2013; Riedel et al., 2014; Osthoff et al., 2008). Due to their significant impacts on radiative forcing, rates of chemical cycling, and the health of living organisms, it is critical to quantify and understand sources of atmospheric Cl radicals.

Sea salt aerosol particles are the largest reservoir of reactive atmospheric Cl. Keene et al. (1999) estimated that at any given time there are ~22 Tg of reactive Cl in the troposphere, and that 68% of this mass is found in particulate form, primarily sea salt. [More recently, Wang et al. \(2021\) suggested there are 2.44 Tg of reactive tropospheric Cl with 90% in particulate form as sea salt. The fact that estimates for the reactive tropospheric Cl budget have decreased by an order of magnitude over the past two decades motivates continued research on tropospheric halogen chemistry and its impacts.](#) Although the Cl in sea salt will not directly photolyze to produce Cl radicals, it can be displaced by acidic species (e.g., sulfate [SO₄²⁻], nitrate [NO₃⁻], organic acids) and released in a reactive gaseous form (e.g., ClNO₂, HCl, Cl₂) that has the potential to produce Cl radicals. This phenomenon is called chloride (Cl⁻) depletion and can be generalized with the following reaction:



where A is one of the acidic species mentioned above. [Note that most of the generated HCl is removed by deposition, but a fraction](#) (~16% globally; Wang et al., 2021) [reacts with OH to produce Cl radicals, which initiates rapid cycling between these radicals and their inorganic non-radical reservoirs.](#) In addition to producing reactive chlorine-containing gases, Cl⁻ depletion can alter the acidity (e.g., Keene and Savoie, 1998), hygroscopicity (e.g., Drozd et al., 2014; Ghorai et al., 2014; Randles et al., 2004), and optical properties (Finlayson-Pitts and Pitts, 2000; Tang et al., 1997) of sea salt particles. Such changes affect partitioning of other chemicals (e.g., water vapor, ammonia [NH₃], SO₄²⁻, NO₃⁻) between the gas and particle phases (Chen et al., 2021), the rates

84 and types of reactions occurring within sea salt particles (Chameides and Stelson, 1993), the
85 activity of these particles as cloud condensation nuclei (e.g., Chatterjee et al., 2020), and their
86 interactions with solar radiation, all of which can have implications for visibility, air quality,
87 biogeochemical cycles, and Earth's radiation budget.

88 Many factors dictate the extent to which Cl^- depletion occurs in an air mass including
89 meteorology (e.g., wind speed, temperature, relative humidity [RH], available solar radiation), the
90 size distribution and mixing state of sea salt particles, and the availability and length of exposure
91 to surrounding acidic species (Su et al., 2022 and references therein). Regarding the latter, Cl^-
92 depletion is therefore typically observed where marine particles and acidic species are both
93 present, such as where emissions from biomass burning (BB) advect over a marine location (Braun
94 et al., 2017; Maudlin et al., 2015; Li et al., 2003; Yokelson et al., 2009; Akagi et al., 2013; Dang
95 et al., 2022; Crosbie et al., 2022), in regions with active phytoplankton and marine bacteria that
96 emit dimethyl sulfide (DMS), which can oxidize to form sulfuric acid (H_2SO_4 ; Seinfeld and Pandis,
97 2016; Tang et al., 2019; Yan et al., 2020), and/or in and around urban coastal environments (e.g.,
98 Kong et al., 2014; Chatterjee et al., 2020; AzadiAghdam et al., 2019; Nolte et al., 2008) where
99 anthropogenic emissions serve as precursors for various acidic species.

100 For this reason, the northwest Atlantic (NWA) is an opportune region for observing and
101 studying Cl^- depletion. Cities extending along the East Coast of North America consistently emit
102 sulfur dioxide (SO_2), nitrogen oxides (NO_x), and VOCs, which can oxidize to form H_2SO_4 , nitric
103 acid (HNO_3), and organic acids, respectively, while sea salt particles are ubiquitous over the region
104 due to wave breaking (Reid et al., 2001; Ferrare et al., 2023). Occasional long-range transport from
105 BB in Alaska, Canada, and the western United States (U.S.; Fehsenfeld et al., 2006; Mardi et al.,
106 2021), agricultural fires throughout the eastern and southeastern U.S. (Jaffe et al., 2020; McCarty
107 et al., 2007), wintertime wood burning for residential heating (Corral et al., 2021; Sullivan et al.,
108 2019), and seasonally varying emissions from vegetation and ocean biological activity (Savoie et
109 al., 2002; Corral et al., 2022) can also introduce acidic species to this region.

110 Cl^- depletion has been observed over the NWA for decades (Table 1). Previous datasets
111 typically span 2 – 3 months, and most are reflective of conditions during the boreal summer,
112 although there are a handful of studies extending outside of this period (i.e., Keene et al., 1990;
113 Yao and Zhang, 2012; Zhao and Gao, 2008; Haskins et al., 2018). Combining results from these
114 works to build seasonal and temporal statistics is challenged by the fact that each dataset is specific
115 to a certain altitude (or range of altitudes), location(s), time period, sampling method, and size
116 range of sampled particles. In addition to these logistical constraints, there is an overall shortage
117 of Cl^- depletion data for the spring, fall and winter, which is of concern as depletion processes are
118 sensitive to several properties that fluctuate seasonally over the NWA (e.g., temperature, solar
119 radiation, RH).

120 Most past works over the NWA report on Cl^- depletion along the United States East Coast
121 (USEC) and/or at Bermuda. To our knowledge, there is an absence of discussion about the gradient
122 in Cl^- depletion moving from the USEC to the open ocean environment closer to Bermuda. Corral
123 et al. (2021) showed strong gradients in aerosol optical depth along this direction for several
124 particle types including sea salt and SO_4^{2-} , suggesting there may be a gradient in Cl^- depletion as
125 well. Furthermore, Cl^- depletion results from previous studies typically reflect conditions near the
126 surface, yet Shinozuka et al. (2004) showed that the vertical scattering profile of sea salt in the
127 lower 1 km of the atmosphere becomes increasingly less uniform with increasing wind speed. Also
128 of note is that most datasets referenced in Table 1 are now several decades old. Mass
129 concentrations of SO_2 , NO_x , SO_4^{2-} , and NO_3^- over the eastern U.S. and Canada have steadily

130 decreased since 1990 due, in part, to the Clean Air Act of 1963 and its subsequent amendments
131 (Feng et al., 2020; Kuklinska et al., 2015). Such reductions warrant an updated analysis of Cl⁻
132 depletion over the NWA.

133 We note that Cl⁻ depletion results from the Wintertime Investigation of Transport, Emissions
134 and Reactivity (WINTER) aircraft campaign (Haskins et al., 2018) are an exception to many of
135 the points raised above. As an airborne campaign from February – March 2015, WINTER provides
136 data relevant to halogen chemistry at altitudes throughout the boundary layer, at a time of year that
137 had previously not been studied, and in a year recent enough to capture the aforementioned
138 reductions in anthropogenically sourced acidic species. However, WINTER flights specifically
139 sampled over and downwind of various pollution sources in the eastern and southeastern U.S.,
140 meaning Cl⁻ depletion results may be disproportionately reflective of highly polluted, coastally
141 influenced air masses as compared to other air mass types observed over the NWA during winter
142 and spring (e.g., those (i) occurring after synoptically forced frontal systems have moved through,
143 (ii) associated with cold air outbreaks (CAOs), and (iii) occurring when southerly winds advect
144 maritime air masses northward along the East Coast).

145 It is common for Cl⁻ depletion studies to base their calculations on the assumption that sea salt
146 particles are the only source of atmospheric sodium (Na⁺; i.e., Na⁺ is used as the reference species
147 for determining the extent of Cl⁻ depletion observed), including nearly all the works listed in Table
148 1. The validity of this assumption is dependent on several factors, including the proximity to urban
149 emissions, if dust particles are present, and the size range of particles sampled. Ooki et al. (2002)
150 found Na⁺ to be highly correlated with potassium (K⁺) in particles < 1.1 μm in urban air masses,
151 implying that these two species have the same source in fine, anthropogenically sourced particles.
152 K⁺ is thought to come mainly from BB (Echalar et al., 1995; Andreae et al., 1998; Andreae and
153 Merlet, 2001) and anthropogenic activities (Ooki et al., 2002 and references therein), suggesting
154 that marine air masses heavily influenced by BB or urban emissions may have nonnegligible
155 contributions from non-sea salt sources to total Na⁺, especially if submicron particles contribute
156 significantly to total mass concentrations (which would depend on the size range of particles
157 sampled). Na⁺ can also be found in mineral dust (Seinfeld and Pandis, 2016), which has motivated
158 a handful of studies to discern between the amounts of Na⁺ coming from dust and sea salt using a
159 system of equations (e.g., Boreddy and Kawamura, 2015; AzadiAghdam et al., 2019). The NWA
160 is known to be periodically influenced by Asian, African, and North American dust (e.g., Aldhaif
161 et al., 2020) and emissions from BB (Fehsenfeld et al., 2006; Schroder et al., 2018; Sullivan et al.,
162 2019; Mardi et al., 2021), and is consistently influenced by anthropogenic activities throughout
163 the year. Several works shown in Table 1 have acknowledged that these additional sources of Na⁺
164 may influence estimates of Cl⁻ depletion over the NWA, but none have quantitatively explored this
165 possibility.

166 Finally, most Cl⁻ depletion studies report the percentage of Cl⁻ in unreacted sea salt particles
167 that has been displaced by acidic species, an approach useful for quantifying the extent of Cl⁻
168 depletion processes independently of the sea salt mass concentrations present, which can vary
169 seasonally, temporally, and geographically. However, reporting Cl⁻ depletion as a percentage can
170 make it more difficult to conceptualize and quantify the degree to which depletion reactions may
171 be affecting atmospheric oxidation potential. Several past works focusing on the NWA have
172 reported the magnitude of Cl⁻ displaced from sea salt particles, either in units of nmol m⁻³ (e.g.,
173 Keene and Savoie, 1998; Keene et al., 1990) or pptv (Keene et al., 2007; Haskins et al., 2018),
174 which we find useful for comprehensive interpretation considering that Singh and Kasting (1988)
175 suggested ppbv concentrations of ~~gaseous and reactive Cl⁻ species (e.g., HCl)~~ have the potential to

176 produce enough Cl radicals to oxidize 20 – 40% of nonmethane alkanes in the marine troposphere.
177 Thus, reporting Cl⁻ depletion both as a percentage and as a mass concentration benefits the
178 atmospheric chemistry community as results can be used either comparatively or to improve
179 quantification of Cl radical budgets and the atmospheric oxidation capacity in a given region.
180 Although a few past works in the NWA have reported mass concentrations of displaced Cl⁻, there
181 is still a need for results reflecting current conditions across a range of seasons as we have
182 discussed above.

183 In summary, there is a demand for an updated, multi-seasonal, spatially resolved dataset
184 reflecting Cl⁻ depletion processes in the NWA boundary layer across a variety of meteorological
185 conditions and air mass types. There is also interest in (i) exploring the sensitivity of Cl⁻ depletion
186 results to accounting for non-sea salt sources of Na⁺, especially in seasons and/or air masses
187 influenced by dust and BB emissions, as well as (ii) quantifying both the percentage and magnitude
188 of Cl⁻ displaced from sea salt particles for straightforward comparisons to other works and to link
189 results more easily to boundary layer Cl radical budgets and their potential influence on
190 atmospheric oxidation rates. This study seeks to address these points by using data from the NASA
191 Aerosol Cloud meTeorology Interactions oVer the western ATlantic Experiment (ACTIVATE)
192 airborne field campaign (Sorooshian et al., 2019). The statistical approach, large number of flights
193 spanning a range of seasons and meteorological conditions, and type of instruments deployed on
194 this campaign make the ACTIVATE dataset well-suited to address several of the outstanding
195 uncertainties and unknowns regarding Cl⁻ depletion over the NWA.

196 **Table 1.** Relevant information from previous works, sorted chronologically, documenting Cl⁻
 197 depletion over the Northwest Atlantic (NWA). “USEC” stands for United States East Coast, and
 198 “U.S.” stands for United States.

Reference(s)	Dates	Location	Platform(s)	Reference species to determine Cl ⁻ depletion	Discusses possibility of non-sea salt sources of Na ⁺ and/or Cl ⁻
Keene et al. (1990)	Jul – Sep 1988	USEC and near Bermuda	Ship and aircraft	Na ⁺	No
Keene and Savoie (1998)	Apr – May 1996	Bermuda	Surface station	Na ⁺	No
Nolte et al. (2008)	May – Jun 2002	Tampa, Florida (U.S.)	Surface stations	Na ⁺	Yes
Yao and Zhang (2012)	Jun – Jul 2002, Oct – Nov 2002	Kejimikujik, Nova Scotia	Surface station	Na ⁺	No
Keene et al. (2004)	Jul – Aug 2002	USEC	Ship	Mg ²⁺ , ²	No
Quinn and Bates (2005)	Jul – Aug 2002	USEC	Ship	Na ⁺	No
Keene et al. (2007)	Jul – Aug 2004	Appledore Island, Maine (U.S.)	Surface station	Na ⁺ and Mg ²⁺	Yes
Zhao and Gao (2008)	Jul – Sep 2006	Newark, New Jersey (U.S.)	Surface station	Na ⁺	Yes
Bondy et al. (2017)	Jun – Jul 2011	Centreville, Alabama (U.S.)	Surface station	Na ⁺ and Mg ²⁺	Yes
Haskins et al. (2018)	Feb – Mar 2015	USEC and over land around major pollution sources across the eastern U.S. ¹	Aircraft	Na ⁺	Yes

199 ¹The Wintertime Investigation of Transport, Emissions, and Reactivity (WINTER) airborne field
 200 campaign focused on three regions over the U.S.: i) the northeast metropolitan corridor
 201 (encompassing major cities from Boston to Washington D.C.), ii) the Ohio River Valley, and iii)
 202 the Southeast. Research flights also extended over coastal waters to sample polluted air masses
 203 downwind from their sources.

204 ²Magnesium (Mg²⁺) was chosen as the reference species for sea salt in Keene et al. (2004) as Na⁺
 205 had a relatively higher and more variable background in the quartz-fiber sampling media used.

206
207
208
209
210
211
212
213
214
215
216
217
218
219
220
221
222
223
224
225
226
227
228
229
230
231
232
233
234
235
236
237
238
239
240
241
242
243
244
245
246
247
248
249
250
251

2. Data and methods

2.1 ACTIVATE campaign description

The ACTIVATE field campaign focused on characterizing relationships between aerosol particles, meteorology, and marine boundary layer clouds over the NWA using two research aircraft flying in coordination. Operations were based out of NASA Langley Research Center (LaRC), although a multitude of other sites supported various aspects of the project. The high-flying King Air usually flew steadily at ~9 km releasing dropsondes and using a suite of remote sensors to retrieve particle and cloud properties below the aircraft. The low-flying HU-25 Falcon (hereafter referred to as the “Falcon”) made in situ measurements of trace gases, aerosol particle properties, cloud and precipitation properties (if present), and meteorological conditions in and around boundary layer clouds or in clear conditions usually below 3 km.

ACTIVATE placed a high priority on building statistics to fulfill its objectives and address current uncertainties regarding aerosol-cloud interactions and remote sensing capabilities over the NWA. To acquire such statistics, the Falcon and King Air achieved 174 and 168 flights with 574 and 592 total flight hours, respectively, from 2020 – 2022 (note that 162 of these were “joint” flights where the aircraft flew in coordination; Sorooshian et al., 2023). The campaign included multiple seasons, with each aircraft adhering to an intentional and consistent flight strategy throughout, to better constrain the multitude of variables affecting a given clear or cloudy scene. As mentioned above, the King Air flew fixedly at ~9 km regardless of the amount of cloud coverage below. In the presence of low-level (<3 km) clouds, the Falcon conducted “cloud ensembles” by flying 3-minute legs at the following key vertical positions: near the ocean surface (MinAlt; ~150 m), below cloud base, above cloud base, below cloud top, and above cloud top. In the absence of low-level clouds, the Falcon switched to “clear ensembles,” which involved 3-minute legs at MinAlt, ~230 m (an altitude useful for remote sensing validation), and at altitudes falling slightly below and above the boundary layer height (see Fig. 2 in Sorooshian et al. [2023] for an illustration of these ensembles). The campaign was executed over six deployments, which are referred to as Winter 2020 (February – March 2020), Summer 2020 (August – September 2020), Winter 2021 (January – April 2021), Summer 2021 (May – June 2021), Winter 2022 (November 2021 – March 2022), and Summer 2022 (May – June 2022) as recommended in Sorooshian et al. (2023). Note that Winter 2022 includes two months in 2021 but is referred to as “Winter 2022” for simplicity.

2.2 Falcon data

The main instrument providing data for this study is a particle into liquid sampler (PILS; Brechtel Manufacturing Inc. [BMI]) that was operated downstream from an isokinetic Clarke-style shrouded solid double-diffuser inlet (BMI; McNaughton et al., 2007) onboard the Falcon. The PILS grows aerosol particles with diameters of 50 - 5000 nm at ambient RH into droplets large enough to be collected via inertial impaction (Sorooshian et al., 2006; Crosbie et al., 2020). Droplets striking the impaction plate are pumped into vials that are analyzed offline using ion chromatography (IC) to quantify air equivalent mass concentrations of Na⁺, ammonium (NH₄⁺), K⁺, magnesium (Mg²⁺), calcium (Ca²⁺), Cl⁻, NO₃⁻, SO₄²⁻, and oxalate. PILS data are critical to this study due to the instrument’s ability to capture particles containing sea salt, dust, and other refractory species that are largely omitted by the aerosol mass spectrometer (AMS). PILS flowrates were set such that it took 300 - 420 s (5 – 7 minutes) to fill each vial, the minimum duration for collecting enough particle mass to be above speciated detection limits while also meeting injection

252 volume requirements for IC analysis. Note that the time spent collecting one PILS sample is greater
253 than the duration of the individual level legs (~3 minutes) comprising clear and cloudy ensembles.
254 The possibility that each PILS sample could represent atmospheric properties sampled during
255 multiple level legs and/or periods of ascent or descent between level legs impacted our analysis in
256 two ways. First, PILS measurements must be considered as a representation of water-soluble ionic
257 composition throughout the lower 3 km of the atmosphere, meaning they cannot provide vertically
258 resolved information. Second, we exclude PILS data collected during cloudy ensembles to
259 eliminate possible cloud contamination. During cloudy ensembles, it is likely that the Falcon
260 intercepted a cloud within any interval of 5 – 7 minutes, and in doing so, shattered droplets and
261 other cloud artifacts were collected in the awaiting sample vial. Additionally, while flying through
262 clouds, large droplets and ice particles can impact onto the walls within the isokinetic inlet where
263 they may resuspend and, therefore, cause delayed sampling, of larger particles previously caught
264 on these walls.

265 The PILS was operated without upstream acid and base denuders since (1) the removal
266 efficiency for specific relevant gases is not well quantified, (2) it is not known how the removal of
267 gases affects the particle-phase equilibrium for semi-volatile species (e.g., NO₃⁻), and (3) the
268 addition of denuders decreases the transmission efficiency of coarse-mode sea salt particles into
269 the PILS. While there could be a small positive artifact from certain gases (e.g., SO₂, HNO₃), the
270 PILS should be much less sensitive to this issue than filter collection methods with offline
271 analysis, which opened the possibility for soluble gases (e.g., NH₃) to contribute to speciated mass
272 concentrations. However, the absence of a base denuder opened the possibility for NH₃, a highly
273 soluble trace gas, to contribute to particulate NH₄⁺ mass concentrations. During quality control
274 analyses, PILS NH₄⁺ mass concentrations were unjustifiably high in many samples, prompting us
275 to omit this species from this study's analysis. As NH₄⁺ is a critical species for deriving parameters
276 relevant to Cl⁻ depletion, we alternatively use NH₄⁺ mass concentrations from a high-resolution
277 time-of-flight aerosol mass spectrometer (HR-ToF-AMS; Aerodyne; DeCarlo et al., 2008;
278 hereafter referred to as an “AMS”), which provided non-refractory mass concentrations of NH₄⁺
279 (among other species) for particles 60 – 600 nm in diameter at a 30-s time resolution. The AMS
280 additionally provided mass concentrations of spectral markers for organic components, of which
281 we use the tracers for oxygenated organics, *m/z* 44, and methanesulfonic acid (MSA), *m/z* 79. The
282 AMS collection efficiency was set to unity as there was not compelling evidence to lower this
283 value when comparing AMS and PILS SO₄²⁻ mass concentrations. AMS data were filtered to
284 isolate those from clear ensembles and then averaged over the 5- to 7-minute interval for each
285 PILS sample. Due to differences in the size range of the PILS and AMS, NH₄⁺ mass concentrations
286 from the AMS represent a lower limit in this analysis.

287 Horizontal wind speed and static air temperature data were obtained using the Turbulent Air
288 Motion Measurement System (TAMMS; Thornhill et al., 2003) operating at 20 Hz time resolution,
289 while the diode laser hygrometer (DLH; Diskin et al., 2002) supplied water vapor mixing ratios
290 and values of RH at 1 Hz time resolution. A commercial cavity ringdown spectrometer (G2401-
291 m; PICARRO, Inc.) provided carbon monoxide (CO) measurements at 0.4 Hz resolution (DiGangi
292 et al., 2021), which are used to qualitatively compare the extent to which certain seasons were
293 influenced by anthropogenic emissions (Panagi et al., 2020; Naeher et al., 2001; Saide et al., 2011).
294 Data are only considered from clear ensembles for each of the parameters described in this
295 paragraph.

296 The Falcon occasionally intercepted clouds during clear ensembles. During these cloud passes,
297 certain instruments (e.g., the AMS) sampled downstream of a counterflow virtual impactor (CVI;

298 BMI; Shingler et al., 2012) for droplet residual characterization. We removed data collected during
299 periods with active CVI sampling from our analysis for all variables mentioned above.

300

301 **2.3 Deployment selection and season/category classifications**

302 This analysis focuses on data collected during the Winter 2022 and Summer 2022
303 deployments as they cover the largest geographical range over the NWA, thus presenting the best
304 opportunity for studying spatial gradients in Cl^- depletion. During Winter 2022, sampling was
305 extended northward on flights when the Falcon flew to Quonset State Airport in Rhode Island,
306 refueled, and returned to LaRC, an option that was unavailable during the first four deployments
307 due to challenges associated with the COVID-19 pandemic. Summer 2022 is the only deployment
308 to (i) execute “transit flights” (i.e., flights where the Falcon flew to Bermuda, refueled, and flew
309 back to LaRC on the same day) and (ii) include a set of out-and-back flights based in Bermuda.
310 Additionally, Winter 2022 and Summer 2022 supply the largest and most continuous dataset
311 compared to the first two years of the campaign. Nearly half of the total Falcon flights occurred
312 within these two deployments, and sampling occurred consistently from 31 November 2021 to 18
313 June 2022 with a brief break from 30 March – 02 May 2022. The high frequency of flights over a
314 ~7-month period allows us to explore the seasonal evolution of properties relevant to Cl^- depletion,
315 while also observing their fluctuations on daily to multiday time scales.

316 To capture both seasonal and spatial trends, Winter 2022 and Summer 2022 data are distributed
317 among the following categories by season/month and/or by the geographical area sampled:
318 December-February (30 November 2021 – 26 February 2022), March (02 – 29 March 2022), May
319 (03 – 20 May 2022), March transit (22 March 2022), May transit (18, 21, and 31 May 2022), and
320 June Bermuda (02 – 13 June 2022). Note that some flights from the Winter 2022 and Summer
321 2022 deployments are omitted from this study because they are either composed entirely of cloudy
322 ensembles and/or PILS data are unavailable during the clear ensembles. To explore relationships
323 between (i) speciated mass concentrations and Cl^- depletion, and (ii) phenomena occurring on finer
324 time scales (e.g., the passage of weather fronts, transport events of African dust plumes),
325 meteorological conditions and/or notable influence from distinct aerosol types are documented for
326 each research flight (RF). We also select RFs sampling various airstreams associated with passing
327 frontal systems and dust-influenced air masses to further illustrate relationships between these
328 phenomenon and properties relevant to Cl^- depletion.

329

330 **2.4 Calculations relevant to Cl^- depletion**

331 The following section describes how various properties associated with Cl^- depletion were
332 derived using PILS and AMS bulk speciated mass concentrations and literature-based ratios for
333 ions in sea salt, dust, and emissions from various combustion processes. Identifying the amount of
334 Cl^- displaced from sea salt particle begins with quantifying the original amount of Cl^- , which we
335 derive from Na^+ in sea salt (ssNa^+) as this species has a relatively high mass fraction and is
336 chemically inert in sea salt particles. We use Eqs. 1 – 5 to resolve contributions of sea salt and dust
337 to bulk PILS mass concentrations of Na^+ and Ca^{2+} (see Sect. S1 in the Supplement for additional
338 information about these equations, Table S1 for variable nomenclature, and Table S2 for values of
339 constant parameters [e.g., mass ratios]).

340

$$Na_{bulk}^+ = ssNa^+ + Na_{dust}^+ \quad 1$$

$$Ca_{bulk}^{2+} = ssCa^{2+} + Ca_{dust}^{2+} \quad 2$$

$$ssCa^{2+} = ssNa^+ \cdot \left(\frac{Ca^{2+}}{Na^+}\right)_{ss} \quad 3$$

$$Ca_{dust}^{2+} = Na_{dust}^+ \cdot \left(\frac{Ca^{2+}}{Na^+}\right)_{dust} \quad 4$$

$$ssNa^+ = \frac{Ca_{bulk}^{2+} - Na_{bulk}^+ \cdot \left(\frac{Ca^{2+}}{Na^+}\right)_{dust}}{\left(\frac{Ca^{2+}}{Na^+}\right)_{ss} - \left(\frac{Ca^{2+}}{Na^+}\right)_{dust}} \quad 5$$

341 We then use an analogous set of equations (Eqs. 6 – 14) to explore if various combustion
 342 processes contribute nonnegligible amounts of Na^+ to bulk PILS Na^+ mass concentrations (see
 343 Sect. S2 for more information).

$$Na_{bulk}^+ = ssNa^+ + Na_{dust}^+ + Na_{comb}^+ \quad 6$$

$$Ca_{bulk}^{2+} = ssCa^{2+} + Ca_{dust}^{2+} \quad 7$$

$$K_{bulk}^+ = ssK^+ + K_{dust}^+ + K_{comb}^+ \quad 8$$

$$ssCa^{2+} = ssNa^+ \cdot \left(\frac{Ca^{2+}}{Na^+}\right)_{ss} \quad 9$$

$$Ca_{dust}^{2+} = Na_{dust}^+ \cdot \left(\frac{Ca^{2+}}{Na^+}\right)_{dust} \quad 10$$

$$ssK^+ = ssNa^+ \cdot \left(\frac{K^+}{Na^+}\right)_{ss} \quad 11$$

$$K_{dust}^+ = Ca_{dust}^{2+} \cdot \left(\frac{K^+}{Ca^{2+}}\right)_{dust} \quad 12$$

$$Na_{comb}^+ = K_{comb}^+ \cdot \left(\frac{Na^+}{K^+}\right)_{comb} \quad 13$$

$$ssNa^+ = \frac{Na_{bulk}^+ - K_{bulk}^+ \cdot \left(\frac{Na^+}{K^+}\right)_{comb} + Ca_{bulk}^{2+} \cdot \left[\left(\frac{K^+}{Ca^{2+}}\right)_{dust} \cdot \left(\frac{Na^+}{K^+}\right)_{comb} - \left(\frac{Na^+}{Ca^{2+}}\right)_{dust}\right]}{1 - \left[\left(\frac{Ca^{2+}}{Na^+}\right)_{ss} \cdot \left(\frac{K^+}{Ca^{2+}}\right)_{dust} \cdot \left(\frac{Na^+}{K^+}\right)_{comb}\right] - \left[\left(\frac{K^+}{Na^+}\right)_{ss} \cdot \left(\frac{Na^+}{K^+}\right)_{comb}\right] - \left[\left(\frac{Ca^{2+}}{Na^+}\right)_{ss} \cdot \left(\frac{Na^+}{Ca^{2+}}\right)_{dust}\right]} \quad 14$$

344

345 Combustion-generated particles over the NWA can stem from a range of seasonal and
 346 perennial processes, each with a different Na^+ and K^+ emission factor. We use empirical, literature-
 347 based values of $\left(\frac{Na^+}{K^+}\right)_{comb}$ for particles emitted from the following combustion-related
 348 activities/phenomena: agricultural burning, forest fires, industrial operations, sauna stove wood
 349 burning for residential heating, car driving, and coal burning for electricity generation (Table S3).

350 Note that only one value at a time can be used for $\left(\frac{Na^+}{K^+}\right)_{comb}$ in Eqs. 13 and 14, which forces the
351 assumption that all combustion-generated particles collected in PILS samples are from the same
352 source and/or have the same $\left(\frac{Na^+}{K^+}\right)_{comb}$ value.

353 Mass concentrations of $ssNa^+$ determined either by Eqs. 1 – 5 or Eqs. 6 – 14 are then used to
354 determine sea salt mass concentrations (Eq. 15) as well as quantities relevant to Cl^- depletion (Eqs.
355 16 – 26).

$$Sea\ salt = ssNa^+ \cdot \left(\frac{total\ mass}{Na^+} \right)_{ss} \quad 15$$

$$\%Cl^- \text{ depletion} = 100 \cdot \frac{ssNa^+ \cdot \left(\frac{Cl^-}{Na^+} \right)_{ss} - Cl_{bulk}^-}{ssNa^+ \cdot \left(\frac{Cl^-}{Na^+} \right)_{ss}} \quad 16$$

$$Lost\ Cl^- = ssNa^+ \cdot \left(\frac{Cl^-}{Na^+} \right)_{ss} - Cl_{bulk}^- \quad 17$$

$$Lost\ Cl_{bulk}^- = Na_{bulk}^+ \cdot \left(\frac{Cl^-}{Na^+} \right)_{ss} - Cl_{bulk}^- \quad 18$$

$$Lost\ Cl_{diff}^- = Lost\ Cl_{bulk}^- - Lost\ Cl^- \quad 19$$

$$nssSO_4^{2-} = SO_{4,bulk}^{2-} - ssNa^+ \cdot \left(\frac{SO_4^{2-}}{Na^+} \right)_{ss} \quad 20$$

$$ExSO_4^{2-} = nssSO_4^{2-} - \frac{MW_{SO_4^{2-}}}{MW_{NH_4^+}} \cdot \frac{NH_{4,bulk}^+}{y_{SO_4^{2-}}} \quad 21$$

$$ExNH_4^+ = NH_{4,bulk}^+ - \frac{MW_{NH_4^+}}{MW_{SO_4^{2-}}} \cdot y_{SO_4^{2-}} \cdot nssSO_4^{2-} \quad 22$$

$$ExNO_3^- = NO_{3,bulk}^- - \frac{MW_{NO_3^-}}{MW_{NH_4^+}} \cdot \frac{ExNH_4^+}{y_{NO_3^-}} \quad 23$$

$$Excess\ acidic\ species = ExSO_4^{2-} + ExNO_3^- + oxalate_{bulk} \quad 24$$

$$Lost\ Cl^- \text{ attr. to } A = [A] \cdot y_A \cdot \frac{MW_{Cl^-}}{MW_A} \quad 25$$

$$Lost\ Cl^- \text{ attr. to excess acidic species} = \sum_{A=ExSO_4^{2-}, ExNO_3^-, oxalate_{bulk}} Lost\ Cl^- \text{ attr. to } A \quad 26$$

356

357 We first calculate the percentage of Cl^- originally in sea salt particles that has been displaced
 358 by acidic species ($\%Cl^-$ depletion; Eq. 16) to facilitate comparisons between our results and other
 359 studies. Subsequently, mass concentrations of displaced Cl^- are calculated using two approaches
 360 to explore the effects of accounting for non-sea salt sources of Na^+ : Approach 1 quantifies
 361 displaced Cl^- using derived mass concentrations of $ssNa^+$ (lost Cl^- ; Eq. 17), while Approach 2
 362 determines displaced Cl^- using bulk PILS Na^+ mass concentrations (lost Cl_{bulk}^- ; Eq. 18), thus
 363 assuming sea salt is the only source of Na^+ . Mass concentrations of lost Cl_{bulk}^- will always be
 364 greater than corresponding values of lost Cl^- , and differences between the two (lost Cl_{diff}^- ; Eq. 19)
 365 are used to assess the significance in accounting for non-sea salt sources of Na^+ when evaluating
 366 the extent of Cl^- depletion processes and their potential effects on atmospheric chemistry.

367 As mentioned above, acidic species are responsible for displacing Cl^- from sea salt particles.
368 However, only a subset of the bulk PILS mass concentrations of SO_4^{2-} and NO_3^- are available for
369 Cl^- depletion reactions, as (i) SO_4^{2-} is a naturally occurring component of sea salt and (ii) available
370 NH_4^+ will neutralize certain amounts of SO_4^{2-} and potentially NO_3^- , leaving them relatively
371 unreactive. Equations 20 – 23 determine mass concentrations of non-sea salt, unneutralized SO_4^{2-}
372 , and NO_3^- , which are added to bulk PILS mass concentrations of oxalate to quantify the amount
373 of excess acidic species (Eq. 24) available for displacing Cl^- from sea salt particles. Note that we
374 use oxalate here as a proxy variable to represent organic acids in general as it is typically the most
375 abundant organic acid in tropospheric aerosol particles (e.g., Hilario et al., 2021; Ziemba et al.,
376 2011; Cruz et al., 2019). We calculate the theoretical amount of lost Cl^- attributable to each excess
377 acidic species (Eq. 25) as well as the total amount attributed to all measured excess acidic species
378 (Eq. 26). Results from Eq. 26 can be compared to values from Eq. 17 to identify the amount of lost
379 Cl^- explained by the measured excess acidic species, and discrepancies in these values may indicate
380 there are additional species contributing to Cl^- depletion (e.g., weak organic acids [Laskin et al.,
381 2012]; reactions initiated by O_3 [Keene et al., 1990]).

382 **2.5 MERRA-2 and NAAPS reanalysis products**

383 Wind speed and wind direction at 950 hPa were obtained from the Modern-Era Retrospective
384 Analysis for Research and Application, Version 2 (MERRA-2; Gelaro et al., 2017) to provide
385 context for large-scale boundary layer wind patterns over the region during each season/category
386 and/or flights of interest. Monthly averages were attained for December 2021 and January,
387 February, March, May, and June 2022 at $0.5^\circ \times 0.625^\circ$ spatial resolution, while 3-hour averages
388 were acquired for periods pertinent to each transit flight as well as the case study flights discussed
389 in Sects. 3.2 and 3.7.1. Monthly averages for December 2021, January 2022, and February 2022
390 were combined and averaged to produce a single wind vector field representative of the December-
391 February category, while averages for March, May, and June 2022 are used to portray conditions
392 for the March, May, and June Bermuda categories, respectively. The 950 hPa pressure layer was
393 selected as this is the Falcon’s median pressure altitude during the Winter 2022 and Summer 2022
394 deployments.

395 We relied on the Navy Aerosol Analysis and Prediction System (NAAPS) to identify the
396 presence of surface-level dust and smoke over the region on selected days using images from the
397 Aerosol Modeling archive (<https://www.nrlmry.navy.mil/aerosol/>) for the “Eastern United States”
398 and “Tropical Atlantic.” We selected images at 1800Z for each day as this time is most relevant to
399 flights during the Winter 2022 and Summer 2022 deployments. NAAPS surface dust and smoke
400 mass concentrations are gridded reanalysis products available at $1^\circ \times 1^\circ$ spatial resolution and 6-
401 hourly temporal resolution, where simulations of dust depend on surface erodible fraction and
402 surface friction velocity (Lynch et al., 2016), and those of smoke depend on size and duration of
403 satellite-detected hotspots (Reid et al., 2009; Hyer et al., 2013). Modeled atmospheric transport of
404 dust and smoke particles is then governed by the Navy Global Environmental Model (NAVGEM;
405 Hogan et al., 2014). These products are used to explore how influence from dust and smoke plumes
406 may affect calculations of Cl^- depletion for case studies presented in Sect. 3.7.1.

407

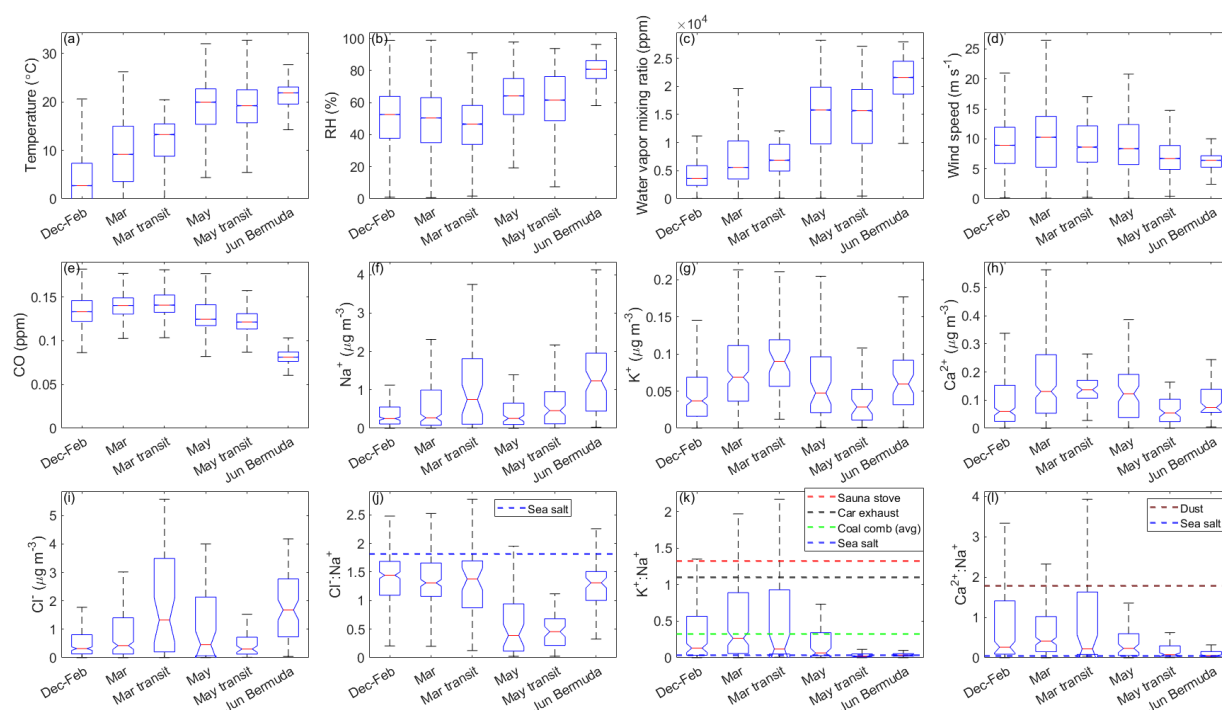
408 **3. Results and discussion**

409 **3.1 Meteorological context**

410 Meteorological conditions during the Winter 2022 and Summer 2022 deployments are mostly
411 consistent with climatological characteristics reported for the NWA in Sorooshian et al. (2020)
412 and Painemal et al. (2021). Median temperatures are lowest in December-February (2.7°C)
413 followed by March (9.2°C), March transit (13.3°C ; recall the March transit flights are in late
414 March), May transit (19.2°C), May (19.9°C), and June Bermuda (21.9°C ; Fig. 1). Median water
415 vapor mixing ratios and RH follow the same trend with the exception that RH slightly decreases
416 from December-February (53%) to March (50%) and March transit (47%). Median wind speeds
417 are highest for March (10.3 m s^{-1}), similar for December-February, March transit, and May (8.9,
418 8.6, and 8.4 m s^{-1} , respectively), and lowest for May transit and June Bermuda (6.7 and 6.4 m s^{-1} ,
419 respectively). MERRA-2 wind fields at 950 hPa (e.g., Fig. 2) show westerly flow along the USEC
420 for December-February that transitions to southwesterly flow for March and March transit, which
421 is a typical progression as the Bermuda High begins to strengthen (Davis et al., 1997). For May
422 and May transit, zonal flow returns north of 34°N while relatively weak southwesterly flow
423 persists to the south. Southwesterly winds dominate for June Bermuda, and large-scale flow
424 patterns across the NWA appear conventional for a fully developed summertime Bermuda High.

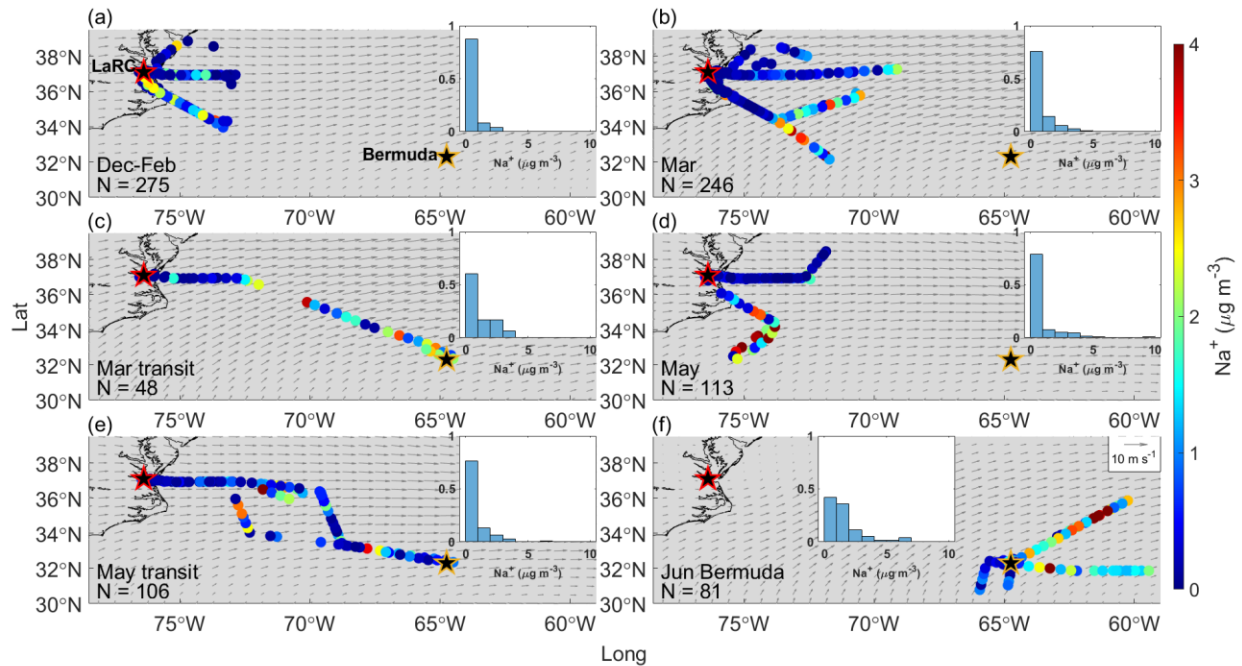
425 Median CO volume mixing ratios are highest for categories sampling solely along the USEC
426 (i.e., December-February [133 ppb], March [141 ppb], and May [124 ppb]) compared to June
427 Bermuda (81 ppb), affirming sampled coastal air masses were most influenced by anthropogenic
428 emissions. We refrain from using CO to compare levels of anthropogenic influence between
429 categories focused on the USEC as CO exhibits seasonal dependence over the NWA (Buchholz et
430 al., 2021). Specifically, peak values are typically observed in early spring due to wintertime
431 accumulation caused by reduced destruction by OH, while increased rates of oxidation by OH over
432 summer lead to minimum concentrations in late summer.

433 Precipitation is considered in this work as (i) wet scavenging processes remove sea salt
434 particles more efficiently than several other particle types (Galloway et al., 1993), and (ii) strong
435 winds associated with precipitation events can enhance sea salt emissions and offset scavenging
436 losses (Dadashazar et al., 2021; Grandey et al., 2011), both of which can influence the amount of
437 Cl^{-} available for depletion reactions on shorter time scales than the seasonal factors discussed
438 above. The NWA receives the most rainfall from December – February followed by June – August,
439 with precipitation rates peaking along the Gulf Stream in all seasons (Painemal et al., 2021).
440 Hawcroft et al. (2012) showed that 65 – 80% and 50 – 70% of the rainfall over the NWA in
441 December – February and June – August, respectively, is associated with midlatitude cyclones
442 (MLC)s, a common year-round weather phenomenon for the region (e.g., Braun et al., 2021;
443 Eichler and Higgins, 2006) largely dictating the eastward transport of trace gases and particulates
444 from North America to the adjacent marine environment (Keim et al., 2005; Cooper et al., 2002,
445 2001). Despite their frequency and known effects on other aerosol properties (e.g., aerosol optical
446 depth and size distribution; Grandey et al., 2011), there is uncertainty in how frontal passages
447 influence parameters relevant to Cl^{-} depletion over the NWA. During this study, meteorological
448 conditions were often driven by MLCs, with synoptic conditions changing every few days (Table
449 2). We discuss key variables in the context of prefrontal and postfrontal airstreams associated with
450 MLCs to explore the influence of midlatitude weather disturbances on depletion reactions and Cl
451 radical budgets over the NWA. Finally, note that clear-ensemble data for December-February do
452 not extend eastward of $\sim 73^{\circ}\text{W}$ due to frequent cloud cover below 3 km over the ocean. This should
453 be taken into consideration when comparing results for December-February to other categories,
454 especially for continentally sourced properties and/or those that depend on wind fetch.



455

456 **Figure 1.** Notched box plots showing seasonal/categorical differences in (a) temperature, (b)
 457 relative humidity (RH), (c) water vapor mixing ratio, (d) wind speed, (e) carbon monoxide (CO)
 458 mixing ratios, bulk mass concentrations from a particle into liquid sampler (PILS) of (f) chloride
 459 (Cl^-), (g) sodium (Na^+), (h) potassium (K^+), and (i) calcium (Ca^{2+}), as well as ratios of these mass
 460 concentrations for (j) $\text{Cl}^-:\text{Na}^+$, (k) $\text{K}^+:\text{Na}^+$, and (l) $\text{Ca}^{2+}:\text{Na}^+$. Data are from clear ensembles only.
 461 Typical ratios for particular ions in sea salt and/or dust are marked with dashed lines in j, k, and l.
 462 In k, we use additional lines to indicate ratios of $\text{K}^+:\text{Na}^+$ reported in the literature for inefficient
 463 batch combustion in a sauna stove (1.33; Lamberg et al., 2011), car exhaust (1.1; Huang et al.,
 464 1994), and coal combustion (0.33; Ondov et al., 1989). The solid red line in the center of each box
 465 indicates the median, box edges represent the 25th and 75th percentiles, and the lower and upper
 466 whiskers indicate the lower limit (first quartile - $1.5 \times$ interquartile range) and upper limit (third
 467 quartile + $1.5 \times$ interquartile range), respectively. The notches span the 95th confidence interval
 468 for the median.



469

470 **Figure 2.** Bulk PILS Na^+ mass concentrations from clear ensembles during (a) December 2021-
 471 February 2022, (b) March 2022, (c) March 2022 transit flights between NASA Langley Research
 472 Center (LaRC; marked with a red-edged star) and Bermuda (marked with a golden-edged star), (d)
 473 May 2022, (e) May 2022 transit flights between LaRC and Bermuda, and (f) the Bermuda field
 474 campaign in June 2022. Normalized histograms in each panel show the distribution of bulk PILS
 475 Na^+ mass concentrations for that specific category since overlap among the colored dots can hide
 476 some from view. Grey arrows indicate the average magnitude and direction of winds at 950 hPa
 477 from MERRA-2 for the period relevant to each category.

478 **Table 2.** Dates, sample quantities, meteorological conditions, and aerosol particle properties
 479 relevant to Cl⁻ depletion for research flights (RFs) considered in each category. Median values of
 480 Na⁺_{bulk} and Ca²⁺_{bulk} are based on bulk PILS data while values of lost Cl⁻, Cl⁻ depletion, and excess
 481 acidic species are derived using Eqs. 1 – 5, 16, 17, and 20 - 24. "N PILS samples" refers to the
 482 total number of PILS samples collected during clear ensembles on the date indicated, while "N_{PILS}"
 483 refers to the number of these samples providing enough information to determine a given property.
 484 "N_{PILS&AMS}" refers to the number of coinciding mass concentrations from the PILS and aerosol
 485 mass spectrometer (AMS) necessary for calculating excess acidic species mass concentrations.

Category	Date	RF(s)	N PILS samples	Meteorological conditions and/or relevant notes	Na ⁺ _{bulk}		Ca ²⁺ _{bulk}		Lost Cl ⁻		Cl ⁻ depletion		Excess acidic species	
					Median (μg m ⁻³)	N _{PILS}	Median (μg m ⁻³)	N _{PILS}	Median (μg m ⁻³ /pptv)	N _{PILS}	Median (%)	N _{PILS}	Median (μg m ⁻³)	N _{PILS & AMS}
Dec-Feb	30 November 2021	94	7	Remains of post-frontal conditions	0.14	7	0.31	7	-0.17/NA ¹	7	0	7	0.29	13
	01 December 2021	95	16	Prefrontal, high pressure; smoke in boundary layer near coast	0.30	16	0.49	16	-0.16/NA ¹	16	0	16	0.59	136
	07 December 2021	96	5	Postfrontal, cold high pressure behind a strong cold front	0.19	5	0.20	5	-0.12/NA ¹	5	0	5	0.03	22
	11 January 2022	100, 101	6	Cold high pressure, cold air outbreak (CAO) conditions	0.34	4	0.05	6	0.12/80	4	20	4	0.49	21
	12 January 2022	102, 103	33	Cold high pressure	0.21	29	0.06	21	0.01/7	15	4	15	0.20	109
	15 January 2022	104	3	Postfrontal	0.63	3	0.05	2	0.01/7	2	4	2	0.35	20
	18 January 2022	105	11	Low pressure moves offshore, sets up CAO conditions	0.22	2	0.06	2	NaN	0	NaN	0	0.01	10
	19 January 2022	107, 108	26	Short-lived high pressure	0.24	14	0.06	10	-0.05/NA ¹	6	0	6	0.14	66
	24 January 2022	109, 110	26	Postfrontal, weak high pressure	0.07	15	0.03	13	-0.04/NA ¹	8	0	8	0.02	86
	26 January 2022	111, 112	20	Postfrontal	0.12	12	0.03	10	0.00/0	7	0	7	0.01	83
	27 January 2022	113, 114	18	Cold high pressure	0.25	16	0.01	5	0.06/40	5	21	5	0.36	41
	01 February 2022	115	8	High pressure	0.90	6	0.05	7	0.41/273	5	21	5	1.00	37
	02 February 2022	116	17	High pressure	0.73	16	0.03	6	0.18/120	6	12	6	0.41	44
	03 February 2022	117, 118	15	High pressure	1.03	14	0.03	5	0.04/27	5	2	5	0.00	10
	15 February 2022	120, 121	34	Postfrontal conditions, cold high pressure	0.25	27	0.03	24	0.08/53	21	17	21	0.56	69
16 February 2022	122, 123	21	Cold high pressure	0.20	18	0.08	20	0.10/67	16	27	16	0.53	105	
19 February 2022	124, 125	38	Weak postfrontal	0.12	30	0.06	37	0.06/40	23	24	23	0.24	186	

	22 February 2022	126, 127	25	Prefrontal, high pressure	1.41	25	0.12	24	0.45/300	24	17	24	0.64	184
	26 February 2022	128, 129	16	Postfrontal	0.13	16	0.06	15	-0.02/NA ¹	15	0	15	0.27	130
	Overall		345		0.25	275	0.06	235	0.04/27	190	6	190	0.30	1372
Mar	02 March 2022	130	39	Postfrontal, high pressure	0.30	36.00	0.16	39	0.04/27	33	8	33	1.20	298
	03 March 2022	131, 132	71	Weak prefrontal	0.91	57.00	0.27	71	0.10/67	57	9	57	1.19	537
	04 March 2022	133, 134	42	Cold high pressure	1.56	40.00	0.12	39	0.42/280	36	14	36	1.02	242
	13 March 2022	138	8	Postfrontal, CAO conditions	0.12	6.00	0.06	7	-0.12/NA ¹	6	0	6	0.02	22
	14 March 2022	139, 140	38	Late postfrontal, cold high pressure; smoke plume sampled from a woodland fire	0.16	37.00	0.06	37	0.03/20	35	13	35	0.22	305
	18 March 2022	141	14	Weak postfrontal	0.18	14.00	0.04	12	0.05/33	12	35	12	0.33	98
	26 March 2022	144, 145	29	Postfrontal; sampled dust, smoke, and potentially pollen	0.05	22.00	0.04	22	-0.02/NA ¹	13	0	13	0.00	147
	28 March 2022	146	17	Postfrontal	0.07	17.00	0.05	12	-0.01/NA ¹	10	0	10	0.13	98
	29 March 2022	147, 148	19	Postfrontal, high pressure, CAO conditions	0.21	17.00	0.05	5	0.02/13	4	34	4	0.00	43
	Overall		277		0.27	246	0.13	244	0.04/27	206	10	206	0.57	1790
May	03 May 2022	149	15	Weak prefrontal; presence of smoke potentially from New Mexico	0.42	15	0.14	12	0.89/594	7	85	7	0.03	92
	05 May 2022	150, 151	18	Postfrontal	0.05	14	0.04	14	0.42/280	2	89	2	0.02	91
	16 May 2022	153, 154	39	Prefrontal to an approaching cold front yet also postfrontal to a departing band of precipitation	0.26	39	0.26	7	0.65/434	1	73	1	0.05	85
	17 May 2022	155	37	Postfrontal	0.08	17	0.01	13	1.53/1020	2	73	2	0.05	52
	20 May 2022	158	28	Warm high pressure, southerly flow due to Bermuda high ² ; haze with potential sampling of bioaerosol	1.75	28	0.17	27	1.91/1274	21	48	21	0.97	148
	Overall		137		0.26	113	0.12	73	1.76/1174	33	64	33	0.05	468
Mar transit	22 March 2022	142, 143	48	High pressure, two days after a cold front and two days before another cold front	0.75	48	0.14	48	0.11/73	43	9	43	0.36	423
May transit	18 May 2022	156, 157	67	Postfrontal along East Coast, aircraft passed across the cold front on the way to Bermuda	0.51	58	0.05	50	1.37/914	31	74	31	0.27	216

	21 May 2022	159, 160	42	Warm high pressure, anticyclonic flow around Bermuda high	0.50	37	0.08	26	1.67/1114	17	75	17	1.87	137
	31 May 2022	161	11	Postfrontal	0.18	11	0.02	5	0.22/147	5	67	5	0.02	20
	Overall		120		0.46	106	0.05	81	1.33/887	53	74	53	0.44	373
Jun Bermuda	02 June 2022	162, 163	4	Prefrontal	0.64	4	0.03	3	0.71/474	2	44	2	2.62	12
	03 June 2022	164	1	Prefrontal, tropical system approaching from the southwest	0.30	1	NaN	0	NaN	0	NaN	0	0.02	1
	05 June 2022	165	29	Could only fly in the morning due to approaching tropical cyclone (TC), TC departs 06 June 2022.	1.76	29	0.08	26	1.35/900	26	36	26	1.97	213
	07 June 2022	167	1	High behind departing TC	2.21	1	NaN	0	NaN	0	NaN	0	0.02	1
	08 June 2022	168, 169	2	High pressure behind TC, African dust known to be in domain	4.28	2	1.07	1	1.12/747	1	11	1	0.04	9
	10 June 2022	170	1	High pressure, isolated thunderstorms, African dust known to be in domain	2.28	1	0.06	1	0.68/454	1	17	1	1.19	9
	11 June 2022	172, 173	20	High pressure, African dust known to be in domain	0.33	20	0.21	12	0.15/100	11	11	11	1.12	71
	13 June 2022	174	25	High pressure, African dust known to be in domain but sampled away from dust for contrast	1.34	23	0.06	24	0.48/320	23	17	23	1.89	170
	Overall		83		1.24	81	0.07	67	0.66/440	64	25	64	1.82	486

486 ¹Negative mass concentrations in $\mu\text{g m}^{-3}$ are reported for lost Cl^- and can be conceptualized as the
487 amount of measured particulate Cl^- in excess of what would be in unreacted sea salt particles based
488 on Eqs. 1 – 4. Negative values may suggest there are additional non-sea salt sources of particulate
489 Cl^- within the sampled air mass. In these cases, we do not provide corresponding gas phase
490 concentrations of lost Cl^- in pptv as these are only meaningful when Cl^- is displaced from sea salt
491 particles.

492 ²Davis et al. (1997)

493 **3.2 Seasonal, spatial, and frontal trends in Na⁺**

494 Cl⁻ depletion studies are motivated by the fact that radicals produced via depletion reactions
495 can influence atmospheric chemistry, the extent to which largely depends on the quantity of
496 radicals generated. Therefore, the amount of Cl⁻ in sea salt available to depletion reactions is
497 critical to quantify, which is why a large portion of our initial discussion is about trends in bulk
498 Na⁺ mass concentrations as they are a reliable indicator of sea salt mass concentrations. Bulk PILS
499 Na⁺ mass concentrations are remarkably similar for December-February, March, and May (median
500 mass concentrations of 0.25, 0.27, and 0.26 $\mu\text{g m}^{-3}$, respectively), higher for March transit and
501 May transit (0.75 and 0.46 $\mu\text{g m}^{-3}$, respectively), and highest in and around Bermuda (1.24 $\mu\text{g m}^{-3}$).
502 In general, past works also typically report higher sea salt mass concentrations in open-ocean
503 environments compared to coastal locations (Table S4), which is intuitive considering that wind
504 fetch is one important factor governing atmospheric sea salt mass concentrations. However, if Na⁺
505 mass concentrations were dictated chiefly by wind fetch over the NWA, values would mostly
506 increase moving eastward, which is not always the case (e.g., Fig. 2e). In fact, there does not appear
507 to be any distinct spatial gradients in Na⁺ mass concentrations for the seasons/categories presented,
508 yet (i) overlap of flight tracks makes it difficult to view all mass concentrations at once, and (ii)
509 we do not have enough data to state that this is always true for the region.

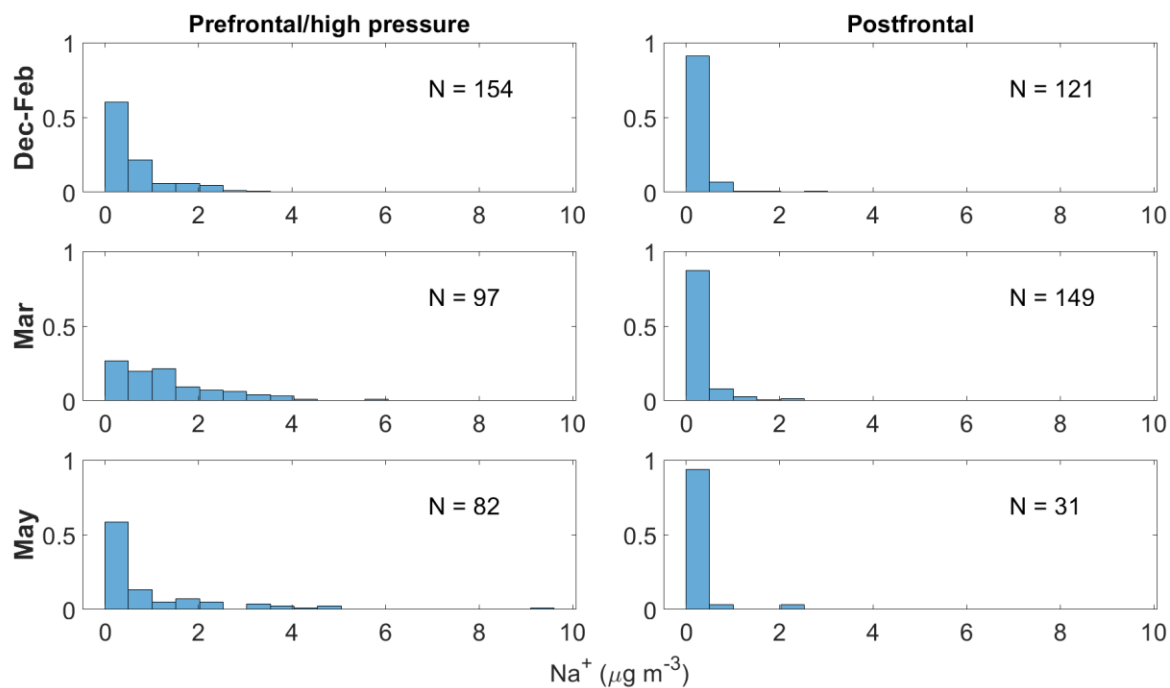
510 Aside from wind fetch, removal via wet scavenging processes is another factor dictating sea
511 salt mass concentrations over marine environments. We explore the effect of passing frontal
512 systems on bulk Na⁺ mass concentrations for December-February, March, and May as (i) bulk Na⁺
513 appears seasonally independent among these categories and (ii) flights sampled the same general
514 region, allowing us to remove coastal versus open-ocean sampling as a confounding variable.
515 When applying the meteorological conditions identified for each day in Table 2, bulk Na⁺ mass
516 concentrations are generally higher during prefrontal/high pressure conditions compared to
517 postfrontal scenes for each seasonal/monthly category (Fig. 3). It is not unusual for bulk Na⁺ mass
518 concentrations to exceed 3 $\mu\text{g m}^{-3}$ in prefrontal and/or high-pressure conditions, especially in
519 March and May, yet values never exceed this threshold in postfrontal conditions. Although bulk
520 statistics suggest frontal passages may reduce sea salt mass concentrations over the NWA, data
521 from prefrontal and postfrontal conditions are not guaranteed to be linked, meaning samples
522 quantifying bulk Na⁺ before and after each frontal passage are not always available. Therefore, we
523 isolate bulk Na⁺ mass concentrations for flights straddling frontal passages to assess the
524 relationship of sea salt mass concentrations and MLCs on a case-study level.

525 Postfrontal conditions on 19 February 2022 (RFs 124 and 125) are associated with bulk Na⁺
526 mass concentrations mostly < 0.3 $\mu\text{g m}^{-3}$ and moderate westerly winds bringing continental air
527 over the NWA (Fig. S1). Three days later (22 February 2022; RFs 126 and 127), prefrontal
528 conditions show increased bulk Na⁺ mass concentrations that are distributed evenly from 0.3 – 2.7
529 $\mu\text{g m}^{-3}$ and southerly winds along the coast. Bulk Na⁺ mass concentrations then swiftly decrease
530 to values mostly below 0.3 $\mu\text{g m}^{-3}$ by 26 February 2022 (RFs 128 and 129) as another MLC moves
531 through the region, although note clear-ensemble sampling was more restricted to the coastline on
532 this day compared to 19 and 22 February 2022.

533 Unfortunately, samples straddling a frontal passage for March are unavailable, but we use
534 consecutive flights from 02 – 04 March 2022 to depict the “recharge” of sea salt mass
535 concentrations following a MLC (Fig. S2). Bulk Na⁺ mass distributions gradually shift towards
536 larger mass concentrations moving from postfrontal conditions with gentle westerly winds (02
537 March 2022; RF 130), to weak prefrontal conditions with stronger northwesterly and southwesterly
538 winds converging at 36 °N (03 March 2022; RFs 131 and 132), and, finally, to cold high-pressure

539 conditions with moderate anticyclonic flow around a high over the northeastern U.S. (04 March
540 2022; RFs 133 and 134). Air masses sampled on 02 and 03 March 2022 appear more continentally
541 influenced and may have been more recently affected by large-scale precipitation compared to the
542 marine air mass sampled on 04 March 2022, which is a potential explanation for the differences in
543 bulk Na⁺ mass concentrations.

544 Flights on 16 May 2022 (RFs 153 and 154) sampled an air mass recently impacted by a
545 retreating band of precipitation yet also considered as prefrontal due to an approaching cold front
546 (Fig. S3). As there was limited time for sea salt mass concentrations to recharge between the
547 consecutive MLCs, it is unsurprising there is little difference in bulk Na⁺ mass concentrations
548 between 16 May 2022 and the postfrontal conditions sampled on 17 May 2022 (RF 155). Frontal
549 influence dissipated by 20 May 2022 (RF 158) with southwesterly flow returning along the
550 coastline in association with the strengthening Bermuda High. This, and the absence of
551 precipitation for several days, may help explain the increase in bulk Na⁺ mass concentrations from
552 mostly below 1 μg m⁻³ on 16 – 17 May 2022 to a mostly above this value on 20 May 2022. The
553 three case studies presented are meant to illustrate how rapidly sea salt mass concentrations can
554 change over the NWA due, in part, to fluctuations in synoptic-scale wind patterns and/or large-
555 scale precipitation associated with MLCs. However, we acknowledge that there are many other
556 confounding atmospheric variables influencing sea salt mass concentrations during these case
557 studies and that flight tracks do not cover the exact same locations on each of these days. Although
558 we do not have enough data to make definitive claims, bulk statistical and case study analyses
559 suggest sea salt mass concentrations decrease behind passing MLCs over the NWA, which
560 corresponds to reduced potential in the amount of reactive chlorine-containing gases that could be
561 produced via depletion reactions compared to in prefrontal and high-pressure conditions.



562

563 **Figure 3.** Normalized histograms showing differences in bulk PILS Na^+ mass concentrations from
 564 clear ensembles occurring in prefrontal and/or high-pressure versus postfrontal conditions for
 565 December-February (top row), March (middle row), and May (bottom row). These categories are
 566 shown as they represent flights occurring in and around the East Coast, eliminating coastal versus
 567 open-ocean sampling as a confounding variable.

568 3.3 Seasonal trends in K⁺, Ca²⁺, Cl⁻ and ion mass ratios

569 As described above, the NWA receives BB emissions from continuous sources (e.g.,
570 fossil fuel combustion for transportation and industrial efforts along the USEC), seasonal practices
571 (e.g., agricultural waste burning in spring, wood burning in winter), and intermittent yet influential
572 events (e.g., forest fires). Using K⁺ as a tracer for such activities, BB influence is greatest during
573 March and March transit flights with median bulk K⁺ mass concentrations of 0.07 and 0.09 μg m⁻³,
574 respectively, compared to 0.04, 0.05, 0.03 and 0.06 μg m⁻³ for the December-February, May,
575 May transit, and June Bermuda categories, respectively. This agrees with previous findings where
576 mass concentrations of organic carbon and particles with diameters 2.5 – 10 μm (PM_{coarse}) were
577 much higher in March than in any other month at a coastal site in Florida (Edwards et al., 2021),
578 and this was attributed mostly to the annual peak in prescribed burning across the southeastern
579 U.S. (Jaffe et al., 2020; McCarty et al., 2007). Our bulk K⁺ mass concentrations are comparable to
580 mean values reported at a receptor site for BB and urban emissions from East Asia (0.02 – 0.05 μg
581 m⁻³; Boreddy and Kawamura, 2015) as well as those in polluted air masses containing dust (0.03
582 μg m⁻³) and biogenically influenced air masses (0.03 μg m⁻³) over the southeastern U.S. during the
583 Study of Emissions and Atmospheric Composition, Clouds, and Climate Coupling by Regional
584 Surveys (SEAC⁴RS; Kacenelenbogen et al., 2022). However, bulk K⁺ values are mostly lower than
585 average K⁺ mass concentrations in air masses influenced by agricultural burning (0.10 μg m⁻³) and
586 wildfire emissions (0.09 μg m⁻³) during SEAC⁴RS (Kacenelenbogen et al., 2022) and also lower
587 than average mass concentrations (0.82 μg m⁻³) measured during the Fire Influence on Regional to
588 Global Environments and Air Quality (FIREX-AQ) airborne field campaign (Adachi et al., 2022)
589 sampling BB plumes in the western and southeastern U.S. Thus, BB particles were consistently
590 present during the Winter 2022 and Summer 2022 deployments, yet relatively dilute compared to
591 their levels in air masses more heavily influenced by BB processes. This is an important point to
592 consider when contemplating how BB emissions may affect estimates of Cl⁻ depletion, which is
593 discussed in greater detail in Sect. 3.7.2.

594 We use bulk Ca²⁺ to identify influence from dust particles and see a similar trend as above
595 where median bulk Ca²⁺ mass concentrations are higher in certain spring categories (0.13, 0.14,
596 and 0.12 μg m⁻³ for the March, March transit, and May categories, respectively) compared to
597 December-February (0.06 μg m⁻³) and June Bermuda (0.07 μg m⁻³). Higher springtime bulk Ca²⁺
598 mass concentrations are likely due to periodic influence from Asian dust plumes, which arrive
599 most frequently over the region from March-May (Aldhaif et al., 2020), and/or to increased
600 suspension of dust particles in BB plumes from agricultural fires across the eastern and
601 southeastern U.S. due to turbulent mixing around flames and the burn front (e.g., Kavouras et al.,
602 2012; Popovicheva et al., 2014; Maudlin et al., 2015; Schlosser et al., 2017; Palmer, 1981).
603 Interestingly, bulk Ca²⁺ mass concentrations are lowest for May transit (0.05 μg m⁻³), but this may
604 be explained by the episodic nature of dust events over the NWA (e.g., Wu et al., 2015; Perry et
605 al., 1997; Prospero, 1999) and the fact that this category is comprised of only three days. African
606 dust plumes become more common over the NWA from June-August (Zuidema et al., 2019) with
607 the strengthening of the Bermuda High, yet the Summer 2022 deployment ended just as these
608 plumes were becoming evident over the region (see meteorological notes for 10, 11, and 13 June
609 2022 in Table 2). There does not appear to be distinct spatial trends in bulk Ca²⁺ over the region
610 for most categories (Fig. S4), presumably as fluctuations in bulk Ca²⁺ may be largely driven by
611 periodic influence from long-range dust transport, smoke plumes from fires along the USEC
612 advecting over the ocean, and midlatitude weather disturbances (Fig. S5). However, a gradient
613 seems to exist along the March transit flights (RFs 142 and 143 on 22 March 2022) such that bulk

614 Ca^{2+} mass concentrations are highest to the east of LaRC and then decrease to the southeast
615 towards Bermuda. This potential sampling of a dust plume and its implications on calculations
616 relevant to Cl^- depletion are explored further in Sect. 3.7.1.

617 Median Cl^- mass concentrations exhibit slightly different seasonal trends than bulk Na^+ , with
618 values lowest for May transit ($0.31 \mu\text{g m}^{-3}$), slightly higher for December-February, March, and
619 May (0.32 , 0.43 , and $0.46 \mu\text{g m}^{-3}$, respectively), and much higher for March transit and Bermuda
620 (1.33 and $1.68 \mu\text{g m}^{-3}$, respectively). The fact that May transit has the third highest median bulk
621 Na^+ mass concentration yet the lowest Cl^- median is the main difference in seasonal trends between
622 these species, which may seem to suggest Cl^- depletion processes are most active for May transit.
623 However, the number of PILS samples providing (i) bulk Na^+ and (ii) Cl^- mass concentrations are
624 very different for May (113 and 43, respectively) and May transit (106 and 65, respectively), yet
625 comparable for December-February, March, March transit, and June Bermuda (Table S5). Thus,
626 it is best to avoid drawing conclusions about Cl^- depletion from individual trends in bulk Na^+ and
627 Cl^- , and to instead focus on samples providing mass concentrations for both species. These samples
628 were isolated to generate the statistics shown in Fig. 1j, which (i) can be considered as a precursory
629 analysis for Cl^- depletion over the NWA where sea salt is assumed to be the only source of Na^+ ,
630 and (ii) are directly comparable to many past works making this assumption. Ratios of $\text{Cl}^-:\text{Na}^+$ are
631 below 1.81 for all categories, suggesting Cl^- depletion processes are consistently occurring over
632 the region. However, median values are much lower for May (0.39) and May transit (0.46)
633 compared to December-February (1.44), March (1.31), March transit (1.38), and June Bermuda
634 (1.31), suggesting that depletion reactions are particularly prevalent in late spring. May and May
635 transit ratios are comparable to those previously reported along the USEC (Quinn and Bates, 2005;
636 Nolte et al., 2008; Zhao and Gao, 2008) in late spring and summer, especially for submicron sea
637 salt particles.

638 As mentioned above, $\text{Cl}^-:\text{Na}^+$ ratios are only an appropriate means to illustrate the extent of Cl^-
639 depletion if sea salt is the predominant source of each species. Ratios of bulk $\text{K}^+:\text{Na}^+$ and $\text{Ca}^{2+}:\text{Na}^+$
640 are useful for indicating if other particle types may be contributing to bulk Na^+ concentrations as
641 these ions are present in distinctly different proportions in sea salt, emissions from various
642 combustion processes, and dust particles. Combustion and/or BB activities do not appear to
643 contribute meaningfully to bulk Na^+ for May, May transit, and June Bermuda as $\text{K}^+:\text{Na}^+$ ratios
644 (0.065 , 0.020 , and 0.037 , respectively) are fairly similar to the reference value for sea salt (0.036 ;
645 Seinfeld and Pandis, 2016; Finlayson-Pitts and Pitts, 2000), whereas ratios exceeding this value
646 are observed for December-February (0.132), March (0.267), and March transit (0.119). Table 2
647 indicates smoke was only directly sampled on four days of the Winter 2022 and Summer 2022
648 deployments (01 December 2021, 14 March 2022, 26 March 2022, and 03 May 2022), suggesting
649 increased $\text{K}^+:\text{Na}^+$ ratios for December-February, March, and March transit may have been driven
650 by increased background levels of BB particles over the NWA from widespread and continuous
651 residential wood burning and prescribed agricultural burning in winter and early spring as opposed
652 to acute BB events. All categories have median $\text{Ca}^{2+}:\text{Na}^+$ ratios exceeding the reference value for
653 sea salt (0.038 ; Bowen, 1979; Finlayson-Pitts and Pitts, 2000), with values of 0.412 , 0.261 , 0.233 ,
654 0.219 , 0.075 , and 0.050 for March, December-February, May, March transit, May transit, and June
655 Bermuda, respectively. These results nicely motivate an investigation into how estimates of Cl^-
656 depletion change when eliminating contributions of (i) dust and (ii) both dust and combustion
657 emissions to bulk Na^+ mass concentrations, which are the topics of Sects. 3.7.1 and 3.7.2,
658 respectively.

659

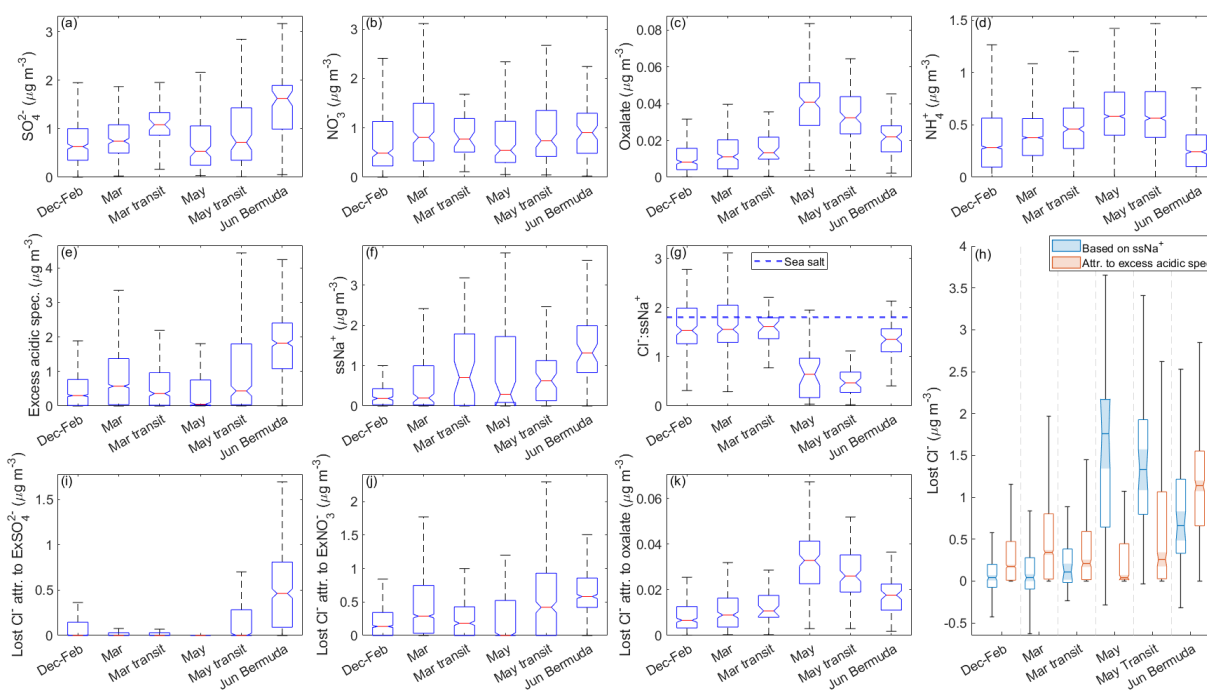
660 3.4 Seasonal, spatial, and frontal trends in acidic species

661 Sea salt mass concentrations alone control the maximum amount of reactive chlorine-
662 containing gases that can be released via Cl^- depletion reactions, but available acidic species are
663 an important factor in regulating the extent to which these reactive gases are actually released.
664 Median mass concentrations of bulk SO_4^{2-} show that this acidic species is a common constituent
665 of sampled air masses, especially for March transit and June Bermuda (Fig. 4; Table S6). Median
666 bulk NO_3^- mass concentrations are of similar magnitude to bulk SO_4^{2-} , yet exhibit less variability
667 among the categories, while oxalate is present in relatively low amounts for December-February,
668 March, and March transit, increases sharply for May and May transit, and then decreases slightly
669 for June Bermuda. In Sect. 2.4, we describe how ssNa^+ mass concentrations and subsequently
670 derived parameters can be calculated either by assuming (i) dust and sea salt or (ii) dust, sea salt,
671 and combustion-sourced particles contribute to bulk Na^+ . In this section and Sects. 3.5, 3.6, 3.7.1,
672 and 3.7.3, we discuss values based on the first assumption, whereas those based on the second
673 assumption are the topic of Sect. 3.7.2.

674 After accounting for contributions of sea salt to SO_4^{2-} and neutralization of non-sea salt SO_4^{2-}
675 and NO_3^- with NH_4^+ , excess SO_4^{2-} (ExSO_4^{2-}) is typically nonexistent for all categories except June
676 Bermuda (median of $0.63 \mu\text{g m}^{-3}$; Fig. S6), while a range of mass concentrations of excess NO_3^-
677 (ExNO_3^-) remain for all categories except May (0.24, 0.51, 0.32, 0.74, $1.02 \mu\text{g m}^{-3}$ for December-
678 February, March, March transit, May transit, and June Bermuda, respectively). Thus, mass
679 concentrations of measured acidic species available to participate in Cl^- depletion reactions are
680 relatively low for May ($0.05 \mu\text{g m}^{-3}$; contributed mostly by oxalate), moderate for December-
681 February, March, March transit, and May transit ($0.30, 0.57, 0.36, 0.44 \mu\text{g m}^{-3}$, respectively), and
682 relatively high for June Bermuda ($1.82 \mu\text{g m}^{-3}$). However, recall that oxalate is used in this study
683 as a proxy for general trends in organic acids, many of which have been shown to considerably
684 displace Cl^- from sea salt particles (e.g., Laskin et al., 2012), including formate, acetate, MSA, and
685 succinate (Kerminen et al., 1998; Braun et al., 2017); thus the results based on oxalate are a lower
686 bound for the effects organic acids have on depletion reactions. Although lower than other aerosol
687 constituents, oxalate mass concentrations are highest for May and May transit along with those of
688 m/z 44, a marker of oxygenated organics that has been shown to correlate with organic acids
689 (Zhang et al., 2005; Takegawa et al., 2007; Sorooshian et al., 2010), and m/z 79, a marker for MSA
690 (Zorn et al., 2008; Van Rooy et al., 2021). Median m/z 44 mass concentrations especially suggest
691 organic acids may play an important role in sea salt particle chemistry for May and May transit as
692 values (0.46 and $0.41 \mu\text{g m}^{-3}$, respectively) (i) are comparable to those of other dominant acidic
693 species over the region, (ii) represent the mass only of the particle fragments (i.e., carboxylic acids)
694 able to displace Cl^- , and (iii) reflect a lower limit of what is actually available for depletion
695 reactions as AMS measurements are for particles 60 – 600 nm.

696 Like sea salt mass concentrations, excess acidic species do not display clear zonal or
697 meridional trends over the NWA (Fig. S7) but do appear to decrease near the USEC following the
698 passage of MLCs (Fig. S8). The reasons are uncertain for such high mass concentrations of excess
699 acidic species for June Bermuda, but a probable cause may be emissions of DMS from marine
700 organisms oxidizing to produce H_2SO_4 (e.g., Luria et al., 1989; Andreae et al., 2003). Excess acidic
701 species mass concentrations are not nearly as high near Bermuda for March transit and May transit
702 compared to June Bermuda, suggesting the increased values in June may be (i) due to greater
703 photochemical production of SO_4^{2-} with increased incident solar radiation (Parungo et al., 1987;
704 Corral et al., 2021) or (ii) due to an episodic surge in local marine biological activity, which has
705 been shown to occur around Bermuda when higher doses of solar radiation become available to

706 the upper mixed layer of the ocean (Vallina and Simó, 2007; Toole and Siegel, 2004). Level-3 (8-
707 day average, 4 km resolution) sea surface chlorophyll a concentrations from MODIS-Aqua show
708 consistent values around Bermuda for March transit, May transit, and June Bermuda. However,
709 there is an important distinction between biomass and ocean biological activity such that steady
710 biomass around Bermuda does not necessarily correspond to similar gaseous emission rates for
711 these categories. Thus, additional research is needed to better understand the seasonal variations
712 in excess acidic species around Bermuda.



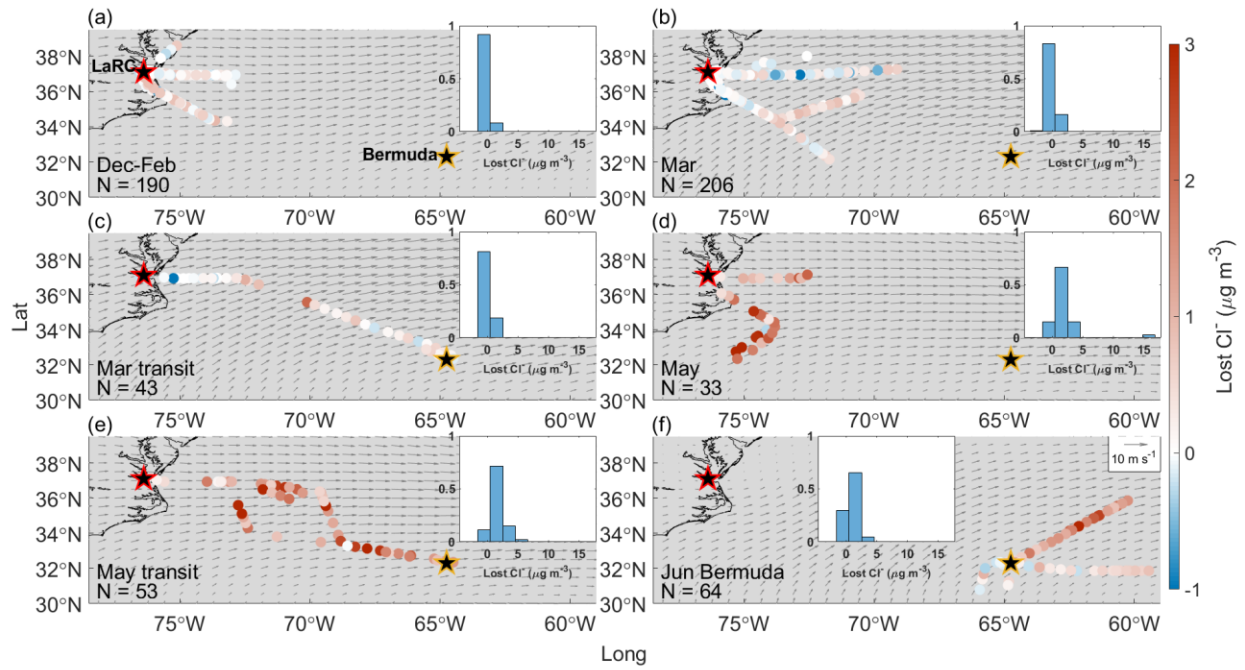
713

714 **Figure 4.** Notched box plots showing seasonal/categorical differences in observed mass
 715 concentrations from clear ensembles of bulk PILS **(a)** sulfate (SO_4^{2-}), **(b)** nitrate (NO_3^-), and **(c)**
 716 oxalate, as well as **(d)** AMS ammonium (NH_4^+). Similar plots are shown for derived mass
 717 concentrations of **(e)** total excess acidic species, **(f)** sea salt Na^+ (ssNa^+), the ratio of **(g)** $\text{Cl}^-:\text{ssNa}^+$,
 718 **(h)** mass concentrations of actual and theoretical lost Cl^- , as well as theoretical mass concentrations
 719 of lost Cl^- attributable to **(i)** excess SO_4^{2-} (ExSO_4^{2-}), **(j)** excess NO_3^- (ExNO_3^-), and **(k)**
 720 oxalate. The value of $\text{Cl}^-:\text{Na}^+$ in sea salt (1.81; Seinfeld and Pandis, 2016) is indicated in **g** with a horizontal
 721 dashed blue line. In **h**, light blue boxes represent the actual Cl^- displaced from sea salt particles
 722 based on derived mass concentrations of ssNa^+ , while light red boxes represent the theoretical
 723 amount of Cl^- that could have been displaced by the derived mass concentrations of excess acidic
 724 species. The properties of the boxes are the same as described in Fig. 1.

725 3.5 Seasonal, spatial, and frontal trends in Cl⁻ depletion

726 Median ssNa⁺ mass concentrations display similar trends to bulk Na⁺ with comparable values
727 among the December-February, March, and May categories (0.19, 0.20, and 0.29 μg m⁻³,
728 respectively), higher mass concentrations for March transit and May transit (0.71 and 0.63 μg m⁻³,
729 respectively), and highest values for June Bermuda (1.32 μg m⁻³). Median ratios of Cl⁻:ssNa⁺
730 (1.54, 1.56, 1.62, 0.65, 0.47, and 1.35 for December-February, March, March transit, May, May
731 transit, and June Bermuda, respectively) are higher than those of Cl⁻:Na⁺ for each category, serving
732 as a preliminary example of how neglecting contributions of dust to bulk Na⁺ can lead to
733 overestimates of Cl⁻ depletion. Regardless of magnitude, Cl⁻:Na⁺ and Cl⁻:ssNa⁺ ratios both convey
734 that the greatest fraction of available sea salt Cl⁻ is converted to reactive chlorine-containing gas
735 during the month of May (i.e., May and May transit categories) over the NWA. Lost Cl⁻ mass
736 concentrations are relatively low for December-February, March, and March transit (0.04, 0.04,
737 and 0.11 μg m⁻³, respectively) then abruptly increase for May and May transit (1.76 and 1.33 μg
738 m⁻³, respectively) followed by a moderate decrease for June Bermuda (0.66 μg m⁻³). These mass
739 concentrations correspond to increases in atmospheric mixing ratios of reactive chlorine-
740 containing gas of 27, 27, 73, 1174, 887, and 440 pptv, respectively, suggesting Cl⁻ depletion
741 processes have the potential to considerably alter rates of boundary layer VOC oxidation in May
742 over the NWA; recall that Singh and Kasting [1998] reported ppbv levels of [such-gasesHCl](#) can
743 produce enough Cl radicals to oxidize 20 – 40% of tropospheric nonmethane alkanes. However,
744 note our reported lost Cl⁻ mass concentrations are for particles with diameters < 5 μm, so although
745 May appears to be the only category where Cl⁻ depletion is severe enough to potentially accelerate
746 tropospheric VOC oxidation, lost Cl⁻ mass concentrations may be higher in reality for other
747 categories, depending on the extent of depletion reactions in larger sea salt particles.

748 There is not a clear spatial gradient in lost Cl⁻ over the region (Fig. 5), but mass concentrations
749 decrease near the USEC after passing frontal systems (Fig. S9), both of which are intuitive as bulk
750 Na⁺ and excess acidic species mass concentrations display the same trends. Although median lost
751 Cl⁻ mass concentrations are above 0 for all categories, negative lost Cl⁻ mass concentrations are
752 observed in 45, 42, 35, 3, 2, and 14% of the samples for December-February, March, March transit,
753 May, May transit, and June Bermuda, respectively. Negative lost Cl⁻ values can be interpreted as
754 there being more Cl⁻ in a sample than expected for unreacted sea salt particles based on derived
755 mass concentrations of ssNa⁺. Such values may indicate influence from non-sea salt sources of Cl⁻
756, such as biomass burning (Jing et al., 2017; Park et al., 2013; Cao et al., 2016), mineral dust
757 (Sullivan et al., 2007), and waste incineration (Moffet et al., 2008). Especially in December-
758 February and March, negative mass concentrations of lost Cl⁻ often occur in samples with
759 relatively high mass concentrations of bulk Ca²⁺ (Fig. S10) and K⁺ (Fig. S11), which can be
760 considered tracers for many of the non-sea salt sources of Cl⁻ mentioned above. However, there
761 are several exceptions to these relationships, and we leave a more thorough investigation into non-
762 sea salt sources of particulate Cl⁻ to future studies.



763

764 **Figure 5.** Same as Fig. 2, except for lost Cl^- .

765 **3.6 Attributing lost Cl⁻ to acidic species**

766 Median mass concentrations of excess acidic species have the potential to displace 0.17, 0.34,
767 0.21, 0.04, 0.26, and 1.14 $\mu\text{g m}^{-3}$ (117, 228, 141, 27, 172, and 758 pptv, respectively) of Cl⁻ from
768 sea salt particles for December-February, March, March transit, May, May transit, and June
769 Bermuda, respectively. These hypothetical losses exceed actual mass concentrations of lost Cl⁻ for
770 all categories except May and May transit, suggesting measured excess acidic species often did
771 not react to their full potential with available particulate Cl⁻, considering median %Cl⁻ depletion
772 values are 6, 10, 9, and 64% for December-February, March, March transit, and June Bermuda,
773 respectively. The extent of depletion reactions in December-February, March, March transit, and
774 June Bermuda may have been limited by meteorological variables (e.g., temperature, RH) and/or
775 restricted access of acidic species to particulate Cl⁻ due to the size distribution and/or mixing state
776 of sea salt particles (Su et al., 2022 and references therein).

777 Most lost Cl⁻ can be attributed mostly to ExNO₃⁻ in December-February, March, March transit,
778 and May transit, which is consistent with findings from past works (e.g., Nolte et al., 2008; Yao
779 and Zhang, 2012; Zhao and Gao, 2008). Excess SO₄²⁻ and ExNO₃⁻ have the potential to contribute
780 equally to Cl⁻ losses for June Bermuda, yet since actual lost Cl⁻ was much lower than theoretical
781 lost Cl⁻, the extent to which each species contributed is unknown. Oxalate has the potential to
782 displace the least Cl⁻ for all categories (0.01, 0.01, 0.01, 0.03, 0.03, and 0.02 $\mu\text{g m}^{-3}$ for December-
783 February, March, March transit, May, May transit, and June Bermuda, respectively), although it
784 is but one organic acid among thousands (Robinson et al., 2007). As mentioned above, there is
785 convincing evidence that organic acids had considerable presence in sampled air masses,
786 especially for Mar transit, May transit and May. This may be due to rising amounts of incident
787 solar radiation accelerating photochemical oxidation of abundant biogenic and anthropogenic
788 VOCs along the USEC to produce secondary organic aerosols (SOA), followed by further
789 oxidation of these SOA to produce oxygenated organics, many of which can serve as weak acids
790 in Cl⁻ depletion reactions. It is possible that unmeasured organic acids are responsible for the lost
791 Cl⁻ that currently cannot be accounted for in May and May transit, although further research is
792 necessary to explore this idea, specifically studies quantifying mass concentrations of additional
793 organic acids in the context of Cl⁻ depletion.

794

795 **3.7 Outcomes from quantifying Cl⁻ depletion semi-unconventionally**

796 In the following subsections we examine the effects of accounting for (i) dust and (ii) dust and
797 combustion emissions as a source of Na⁺, as well as focusing our discussions on mass
798 concentrations of Cl⁻ displaced from sea salt particles instead of either %Cl⁻ depletion or Cl⁻:Na⁺
799 ratios alone. We consider these to be “semi-unconventional” approaches as a handful of studies
800 have employed at least one of these methods, but they are not commonly used in Cl⁻ depletion
801 studies (based on the 76 studies presented in Table S3 in Su et al., 2022). However, we
802 acknowledge many works neglect non-sea salt sources of Na⁺ after determining crustal
803 contributions are unlikely (e.g., Rastogi et al., 2020; Bondy et al., 2017) or avoid calculating Cl⁻
804 depletion for particles of a certain size range when anthropogenic sources seem to contribute to
805 Na⁺ and/or Cl⁻ (e.g., Feng et al., 2017; Nolte et al., 2008). This work builds on past studies to
806 provide an all-encompassing method for quantifying Cl⁻ depletion in air masses influenced by dust
807 and/or combustion emissions, as well as relating Cl⁻ losses to their potential effects on atmospheric
808 oxidation processes. We now discuss when, if ever, these methods are of importance for the NWA
809 and provide a few lessons learned for future works interested in using these methods.

810

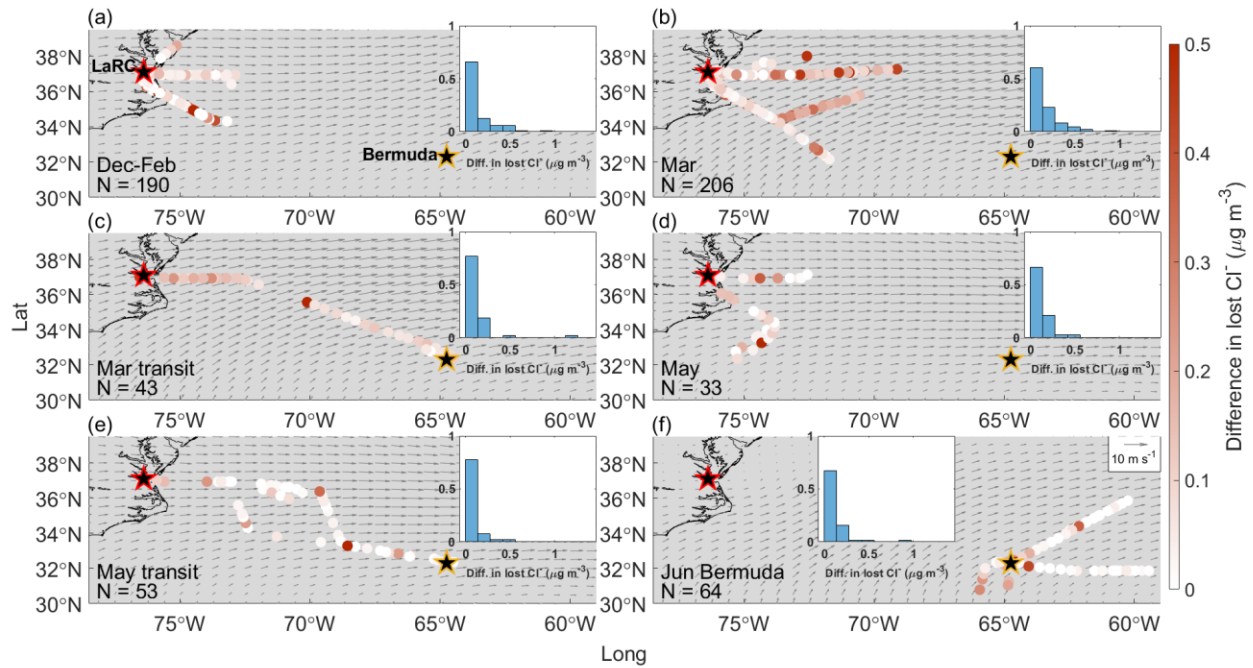
811 3.7.1 Significance of accounting for Na⁺ in dust

812 To facilitate understanding of the results below, recall mass concentrations of lost Cl_{diff}⁻
813 quantify the difference in estimating Cl⁻ depletion when dust is considered as a source of Na⁺
814 (Approach 1) versus when Na⁺ is attributed entirely to sea salt (Approach 2). Median lost Cl_{diff}⁻
815 mass concentrations are 0.05, 0.1, 0.09, 0.05, 0.02, and 0.01 μg m⁻³ (33, 64, 59, 34, 11, and 7 pptv,
816 respectively) for December-February, March, March transit, May, May transit, and June Bermuda,
817 respectively, meaning that Cl⁻ losses are overestimated by a factor of 2.24, 3.38, 1.80, 1.03, 1.01,
818 and 1.01, respectively, when using Approach 2 versus Approach 1. However, even though
819 overestimates are proportionately large for December-February, March, and March transit, it may
820 not be critical to account for dust as a source of Na⁺ on a seasonal scale (Fig. 6). Specifically,
821 lost Cl_{bulk}⁻ mass concentrations for December-February, March, and March transit (58, 91, and
822 133 pptv, respectively) are still well below the point where they would significantly accelerate
823 VOC oxidation in the boundary layer. Similarly, Approaches 1 and 2 both lead to the conclusion
824 that depletion reactions in May have the potential to accelerate tropospheric VOC oxidation, while
825 lost Cl_{diff}⁻ values are too small for May transit and June Bermuda to affect overarching conclusions
826 regarding relationships between Cl⁻ depletion and VOC oxidation rates. However, this study
827 reports mass concentrations of lost Cl⁻ and lost Cl_{diff}⁻ for particles with ambient diameters < 5 μm,
828 so it is possible that contributions of Na⁺ from dust particles > 5 μm may be sufficiently high to
829 lead to critical overestimates in Cl⁻ depletion, especially considering that lost Cl⁻ mass
830 concentrations may increase when additionally accounting for depletion in larger sea salt particles.

831 Although not critically important on a seasonal scale, Approaches 1 and 2 produce
832 considerably different estimates of lost Cl⁻ for several flights sampling air masses more heavily
833 influenced by dust. Median bulk Ca²⁺ mass concentrations are 5.2 and 8.2 times higher on 30
834 November and 01 December 2021 (RFs 94 and 95, respectively) than the December-February
835 median without corresponding enhancements in bulk Na⁺, suggesting a higher presence of dust
836 than usual. Using Approach 1, 100% and 88% (0.14 and 0.23 μg m⁻³, respectively) of median bulk
837 Na⁺ mass concentrations are attributed to dust for 30 November and 01 December (Table S7),
838 respectively, which results in corrections of lost Cl⁻ up to 0.63 μg m⁻³ (420 pptv) compared to
839 overestimates based on Approach 2 (Fig. 7). Dust particles sampled on these flights were likely
840 lofted in smoke plumes extending over the NWA from fires in the eastern and southeastern U.S.
841 On 03 March 2022 (RFS 131 and 132), median bulk Ca²⁺ and Na⁺ mass concentrations are 2.1 and
842 3.4 times higher, respectively, than categorical medians, as it appears the NWA was heavily
843 influenced by BB emissions from agricultural fires throughout the eastern U.S. Although only 15%
844 of the median bulk Na⁺ mass concentration is attributed to dust, lost Cl_{diff}⁻ mass concentrations are
845 as high as 1.05 μg m⁻³ (700 pptv), with most between 0.11 and 0.32 μg m⁻³ (73 - 213 pptv). As
846 mentioned in Sect. 3.3, there is interest in exploring the spatial gradient in bulk Ca²⁺ along March
847 transit flights (RFs 142 and 143) to see how estimates of Cl⁻ depletion are affected by the transition
848 from a potentially dust-influenced air mass (directly east of LaRC) to one with less dust influence
849 (to the southeast towards Bermuda). Although lost Cl_{diff}⁻ mass concentrations are lower compared
850 to those of previous case studies, Approach 2 overestimates Cl⁻ depletion more for the air mass
851 closest to the USEC compared to that closest to Bermuda. The air mass with higher bulk Ca²⁺ mass
852 concentrations appears to be composed of emissions from widespread springtime BB, and the
853 shape of the plume is such over the NWA that the aircraft would fly in it near the USEC but not
854 necessarily near Bermuda. The case studies above suggest that Cl⁻ depletion can be considerably
855 overestimated in smoke plumes when using Approach 2 as entrained dust particles can contribute
856 meaningfully to bulk Na⁺ mass concentrations, and that these overestimates may be of

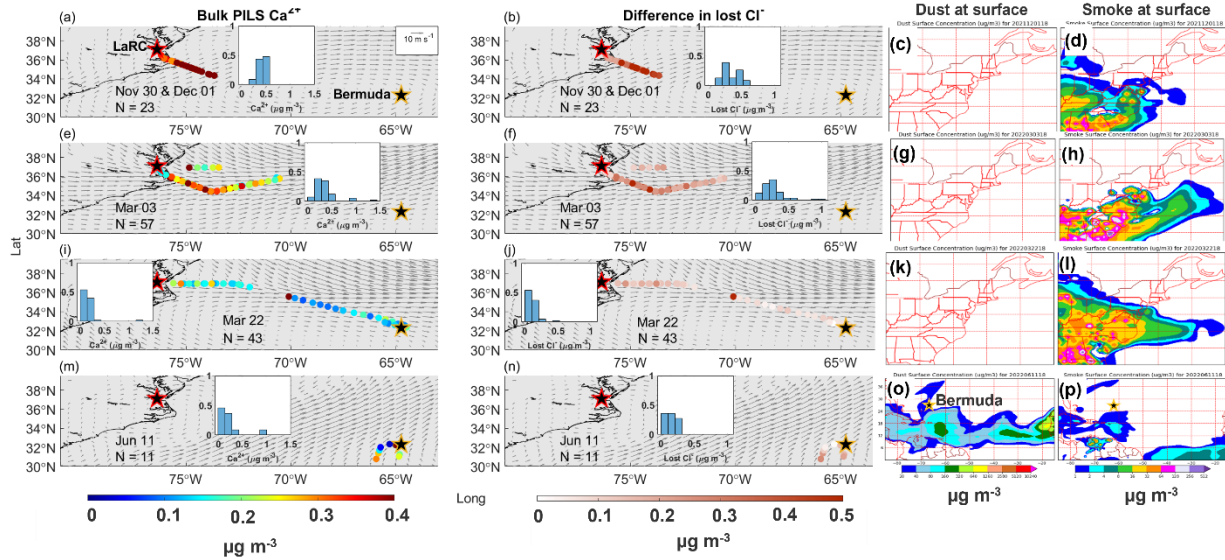
857 consequence when relating Cl^- depletion to potential increases in VOC oxidation over the region.
858 Median Ca^{2+} mass concentrations are 3 times higher ($0.21 \mu\text{g m}^{-3}$) than the June Bermuda median
859 on 11 June 2022 (RFs 172 and 173) without similar enhancements in bulk Na^+ , suggesting
860 increases in bulk Ca^{2+} are likely due to African dust sampling (as opposed to increased sea salt
861 mass concentrations). The arrival of African dust near Bermuda results in overestimates of lost Cl^-
862 up to $0.315 \mu\text{g m}^{-3}$ (210 pptv) via Approach 2, which are not large enough to affect predictions for
863 potential increases in rates of tropospheric VOC oxidation. Sampling ended near the beginning of
864 the peak season for long-range transport of African dust to the NWA (e.g., Prospero, 1996;
865 Zuidema et al., 2019), so we do not have many flights to choose from for studying effects of
866 African dust plumes on Cl^- depletion calculations. Using 6300 ppm as a mass ratio of Na^+ in dust
867 particles (Seinfeld and Pandis, 2016), 131.54 and $73.66 \mu\text{g m}^{-3}$ of dust would be necessary to cause
868 critical overestimates of lost Cl^- (i.e., lost $\text{Cl}_{\text{bulk}}^-$ values would reach $1.5 \mu\text{g m}^{-3}$ using Approach 2)
869 assuming 0 and $0.66 \mu\text{g m}^{-3}$ of Cl^- were already being displaced from sea salt particles, respectively
870 (note $0.66 \mu\text{g m}^{-3}$ is the median lost Cl^- value for June Bermuda). Edwards et al. (2021) reported
871 peak African dust mass concentrations of $73.32 \mu\text{g m}^{-3}$ near Miami, Florida, so it may be possible
872 for values to reach these levels over Bermuda, but it would take a relatively large plume. Therefore,
873 it is typically not critical to use Approach 1 when quantifying Cl^- depletion near Bermuda, yet it
874 may be important to use this approach during strong African dust events.

875 Furthermore, past works have demonstrated the uptake of precursors to acidic species (e.g.,
876 NO_x , SO_2 ; Grassian, 2002; Hanisch and Crowley, 2003; Ullerstam et al., 2002), inorganic acids
877 (e.g., H_2SO_4 , HNO_3 ; Ooki and Uematsu, 2005; Sullivan et al., 2007), organic acids (Al-Hosney et
878 al., 2005; Carlos-Cuellar et al., 2003), and HCl (Zhang and Iwasaka, 2001; Ooki and Uematsu,
879 2005; Sullivan et al., 2007; Santschi and Rossi, 2006; Sorooshian et al., 2012) on dust particles.
880 Thus, in addition to considering dust as a source of Na^+ , it may also be important to account for its
881 presence to avoid overestimating Cl^- depletion and its impacts on atmospheric oxidation as (i)
882 uptake of acidic species and their precursors may reduce amounts available for depletion reactions,
883 and (ii) deposition of HCl on dust particles may reduce the amount of Cl radicals produced
884 following Cl^- displacement.



885

886 **Figure 6.** Same as Fig. 2, except for differences in lost Cl^- when sea salt is assumed to be the only
 887 source of bulk Na^+ versus when sea salt and dust are both considered to contribute to bulk Na^+
 888 mass concentrations.



889

890 **Figure 7.** Spatial relationships between mass concentrations of (a) bulk PILS Ca^{2+} and (b)
 891 differences in lost Cl^- , as well as NAAPS reanalysis surface mass concentrations of (c) dust and
 892 (d) smoke for the case study on 30 November – 01 December 2022 (RFs 94 and 95). The second,
 893 third, and fourth rows correspond to case studies on 03 March (RFs 131 and 132), 22 March (RFs
 894 142 and 143), and 11 June (RFs 172 and 173) 2022, respectively, where (e, f, g, h), (i, j, k, l), and
 895 (m, n, o, p) display the same variables as (a, b, c, d), respectively. Normalized histograms for bulk
 896 PILS Ca^{2+} and differences in lost Cl^- show the distribution of values for that specific case study
 897 since overlap among the colored dots can hide some from view. Grey arrows indicate the average
 898 magnitude and direction of MERRA-2 winds at 950 hPa for the month(s) relevant to each category.
 899 NASA Langley Research Center (LaRC) and Bermuda are marked with red-edged and golden-
 900 edged stars, respectively.

901 **3.7.2 Significance of accounting for Na⁺ in dust and combustion-sourced particles**

902 As shown above, air masses influenced by BB frequently advect over the NWA, especially in
903 March, occasionally increasing dust mass concentrations to levels capable of causing considerable
904 overestimates in Cl⁻ depletion. However, there is little to no effect on Cl⁻ depletion calculations
905 when accounting for contributions to Na⁺ from combustion particles emitted via agricultural
906 burning and forest fires as median Na_{comb}⁺ mass concentrations are 0.00 μg m⁻³ for all categories
907 (Tables S8 and S9, respectively). Therefore, it may be more important to quantify contributions of
908 dust as opposed to the combustion-sourced particles in smoke plumes over the NWA to avoid
909 overestimates of Cl⁻ depletion. However, recall median bulk K⁺ mass concentrations for this study
910 are 2 and 14 times lower than values measured in air masses more heavily influenced by (i)
911 agricultural burning (Kacenenbogen et al., 2022) and (ii) wildfire smoke (Adachi et al., 2022),
912 respectively. Thus, it is possible quantifying Na_{comb}⁺ is important for accurate estimates of Cl⁻
913 depletion in more concentrated BB plumes, yet we cannot explore this with the flights available
914 and leave such an investigation to future studies. When combustion emissions are attributed to
915 industrial operations, residential wood burning in sauna stoves, car driving, or coal burning at
916 power plants, there is also no influence on Cl⁻ depletion calculations for any category (i.e., all
917 median Na_{comb}⁺ values are 0.00 μg m⁻³; Tables S10 – S13). Thus, particles generated by the myriad
918 of combustion processes occurring along the eastern U.S. may be too dilute over the NWA to affect
919 calculations of Cl⁻ depletion not only in air masses reaching Bermuda but also in those much closer
920 to the USEC (e.g., Fig. S12).

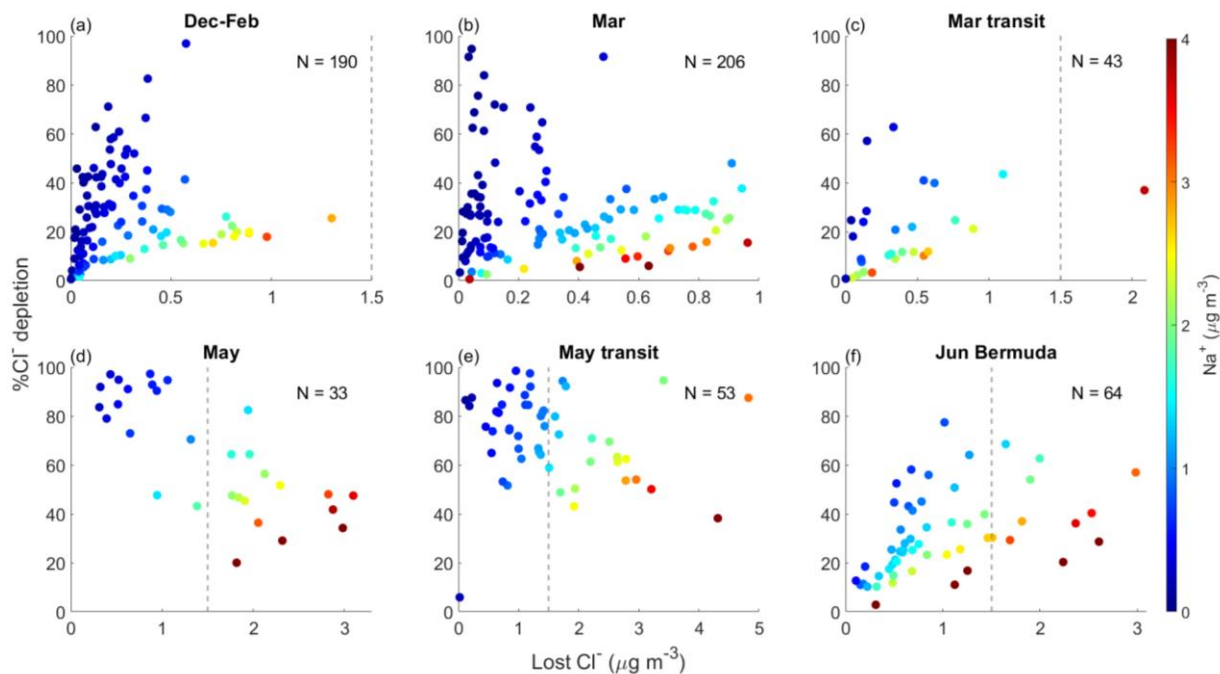
921 Since mass concentrations of Na_{comb}⁺ are typically negligible, Eqs. 1 – 4 and 6 – 13 should
922 provide the same median mass concentrations of ssNa⁺ and Na_{dust}⁺ for each category. However,
923 many samples are excluded when using Eqs. 6 – 13 as their K⁺ mass concentrations are below IC
924 detection limits, causing adjustments in median ssNa⁺ and Na_{dust}⁺ values for several categories.
925 Despite the advantages in accounting for non-sea salt sources of Na⁺, one disadvantage is potential
926 dataset reduction. For example, 275, 246, 48, 113, 106, and 81 samples provide bulk Na⁺ mass
927 concentrations for December-February, March, March transit, May, May transit, and June
928 Bermuda, respectively, yet only 202, 220, 48, 64, 75, and 66, respectively, can be used in Eqs. 1 –
929 4, with even fewer available for use in Eqs. 6 – 13 where concurrent mass concentrations of bulk
930 Na⁺, Ca²⁺, and K⁺ are necessary. Thus, future studies may want to weigh the consequences of
931 neglecting contributions of Na⁺ from non-sea salt sources versus potential reductions to the number
932 of samples included in statistical analyses.

933

934 **3.7.3 Significance of focusing on lost Cl⁻ instead of %Cl⁻ depletion**

935 Values of %Cl⁻ depletion display similar trends to lost Cl⁻ mass concentrations, where most
936 percentages are (i) relatively low for December-February, March, and March transit (half are ≤
937 10%, nearly all are ≤ 50%), (ii) relatively high for May and May transit (nearly all are > 40%),
938 and (iii) relatively moderate for June Bermuda (values are distributed fairly evenly from 0 – 30%,
939 and nearly all are ≤ 60%, Fig. S13). However, these %Cl⁻ depletion values can only be used to
940 show relative seasonal/categorical differences, and they cannot (i) inform when Cl⁻ mass transfer
941 is greatest from the particulate to gas phase or (ii) place such depletion reactions in the context of
942 their potential influence on tropospheric VOC oxidation rates. For example, samples with higher
943 %Cl⁻ depletion values can easily be misinterpreted as having greater Cl⁻ losses when in reality the

944 opposite may be true. Lost Cl^- and % Cl^- depletion have a negative correlation for May and May
945 transit, meaning that samples with the least (most) displaced Cl^- have the highest (lowest) % Cl^-
946 depletion values (Fig. 8). The remaining categories have mostly positive correlations between lost
947 Cl^- and % Cl^- depletion, although % Cl^- depletion values are typically higher for samples with
948 relatively low bulk Na^+ mass concentrations at a fixed lost Cl^- value. This trend may be due to
949 samples containing sea salt particles with varying size distributions (i.e., lower bulk Na^+ mass
950 concentrations may mean smaller sea salt particles were collected in a given sample) and
951 considering that smaller sea salt particles are typically more susceptible to depletion reactions (e.g.,
952 Su et al., 2022 and references therein). However, this behavior may also be an artifact of increased
953 sensitivity of % Cl^- depletion to samples with relatively small ssNa^+ mass concentrations. Many of
954 the samples with mass concentrations of lost Cl^- high enough to potentially influence VOC
955 oxidation rates (i.e., lost $\text{Cl}^- > 1.5 \mu\text{g m}^{-3}$) have % Cl^- depletion values $< 40\%$, while nearly all
956 samples with % Cl^- depletion values $> 80\%$ do not have Cl^- losses capable of affecting such rates.
957 Thus, we highly recommend future studies quantify mass concentrations of lost Cl^- to make results
958 from depletion studies more suitable for understanding mass exchange between sea salt particles
959 and the surrounding atmosphere and the consequences this can have on rates of tropospheric
960 chemistry and radiative forcing.



961

962 **Figure 8.** Relationships between mass concentrations of lost Cl^- and $\% \text{Cl}^-$ depletion for (a)
 963 December-February, (b) March, (c) March transit, (d) May, (e) May transit, and (f) June Bermuda.
 964 Markers are colored by bulk PILS Na^+ mass concentrations, and the vertical dashed gray line in
 965 some panels denotes where mass concentrations of lost Cl^- may begin to have considerable
 966 influence on tropospheric VOC oxidation rates.

967 4. Conclusions

968 This study investigates Cl⁻ depletion in sea salt particles over the NWA from approximately
969 December 2021 – June 2022 using an airborne dataset quantifying the chemical composition of
970 particles < 5 μm among other parameters throughout the lower 3 km of the atmosphere. Trends in
971 bulk PILS Na⁺ suggest sea salt mass concentrations (1) do not exhibit seasonal variation but are
972 reduced following the passage of MLCs near the USEC, and (2) are higher in the open-ocean
973 environment of Bermuda than along the USEC. Losses of Cl⁻ are greatest in May and least in
974 December-February and March, with median lost Cl⁻ mass concentrations of 1.76, 0.04, and 0.04
975 μg m⁻³ (1174, 27, and 27 pptv), respectively. Mass concentrations of measured excess acidic
976 species can account for all the Cl⁻ depletion observed in December-February, March, and June
977 near Bermuda, yet none in May, suggesting unmeasured organic acids may be largely responsible
978 for displacement in certain months. Accounting for dust as a source of Na⁺ is not critical for
979 accurately predicting how Cl⁻ depletion reactions will influence rates of tropospheric VOC
980 oxidation on a seasonal basis, yet this may be important for large smoke and dust plumes over the
981 NWA. Combustion-sourced particles do not contribute enough Na⁺ to meaningfully affect Cl⁻
982 depletion estimates in any season for the air masses sampled. Finally, quantifying Cl⁻ depletion as
983 a percentage sufficiently captures seasonal trends in depletion processes but fails to convey the
984 effects they may have on atmospheric oxidation rates.

985 These results help address several uncertainties regarding Cl⁻ depletion over the NWA and its
986 influence on regional oxidation cycles. First, by identifying factors affecting regional sea salt mass
987 concentrations, we help advance the scientific community towards better understanding and
988 forecasting of regional fluctuations in this major reactive atmospheric Cl reservoir. Additionally,
989 seasonally resolved mass concentrations of lost Cl⁻ reveal that depletion reactions correspond to
990 increases in ~~reactive-chlorine-containing-gases~~HCl capable of producing concentrations of Cl
991 radicals sufficient to oxidize 20 – 40% of nonmethane alkanes in the marine troposphere in May,
992 which can have numerous implications including potentially accelerating O₃ production over this
993 highly populated region. The possibility for dust to cause meaningful overestimates of Cl⁻
994 depletion is a regionally novel finding and should encourage future studies and modeling efforts
995 to monitor and account for smoke and dust plumes advecting over the NWA when quantifying sea
996 salt reactivity. Additionally, our results reveal the importance in quantifying absolute Cl⁻ losses as
997 samples with the highest values of %Cl⁻ depletion often have relatively low Cl⁻ losses, and lost Cl⁻
998 and %Cl⁻ depletion are negatively correlated in May, which is critical to recognize as Cl⁻ depletion
999 has the greatest potential effect on tropospheric VOC oxidation rates during this month compared
1000 to all other studied.

1001 Lost Cl⁻ mass concentrations are similar between median values reported in this study and the
1002 mean presented in Keene et al. (1990) for summertime conditions around Bermuda (0.66 and 0.68
1003 μg m⁻³, respectively), while our values also fall within the range observed over Bermuda in spring
1004 (0.22 – 1.35 μg m⁻³; Keene and Savoie, 1998). Keene et al. (1990) reported lower lost Cl⁻ mass
1005 concentrations along the USEC from July-September than our findings in May (1.11 and 1.76 μg
1006 m⁻³, respectively), while our median in May is above the range shared in Keene et al. (2007) for
1007 July-August (0 – 1.31 μg m⁻³). Haskins et al. (2018) quantified median lost Cl⁻ mass concentrations
1008 of 0.30 μg m⁻³ over the ocean from February – March, which is 7 times higher than our medians
1009 for December-February and March (0.04 and 0.04 μg m⁻³, respectively), yet note their study
1010 specifically targeted polluted winter air masses while ours did not. Many past works along the
1011 North American east coast have been able to attribute Cl⁻ depletion largely to inorganic acids in
1012 the summer and fall (Zhao and Gao, 2008; Keene et al., 2007; Nolte et al., 2008; Yao and Zhang,

1013 2012), with Keene et al. (1990) reporting a lowest contribution of 38%. We can attribute all Cl⁻
1014 depletion to inorganic acids in December-February, March, and June, yet find inorganic acids do
1015 not contribute at all to displacement reactions in May. Our study suggests depletion reactions are
1016 still occurring to the extent they were in the 1990s and 2000s over the NWA except that organic
1017 acids are possibly becoming increasingly responsible for Cl⁻ displacement, especially in May,
1018 although further research is needed to verify this.

1019 Although the ACTIVATE dataset is well-equipped to explore seasonal and spatial trends in
1020 Cl⁻ depletion over the NWA, there are several caveats and limitations to be mindful of when
1021 reviewing our results. Reported mass concentrations of sea salt and lost Cl⁻ should be interpreted
1022 as a lower limit due to the size range of particles sampled (< 5 μm). Additionally, calculations for
1023 the neutralization of SO₄²⁻ and NO₃⁻ by NH₄⁺ combine speciated mass concentrations from two
1024 separate instruments, each considering a different size range of particles, meaning mass
1025 concentrations of excess acidic species should be considered as an upper limit for particles < 5
1026 μm. We recommend accounting for non-sea salt sources of Na⁺ when appropriate but acknowledge
1027 that it may limit statistical analyses as the procedure for disentangling contributions of various
1028 sources to bulk Na⁺ requires synchronous mass concentrations of multiple species.

1029 Overall, this study presents an updated account of sea salt reactivity over the NWA while also
1030 providing unprecedented statistics for (i) responses in parameters relevant to Cl⁻ depletion to
1031 passing frontal systems, (ii) sea salt particle mass concentrations within the lower 3 km of the
1032 atmosphere between the USEC and Bermuda, (iii) the extent of Cl⁻ depletion occurring in a variety
1033 of air masses in winter, spring, and early summer as well as the importance of (iv) accounting for
1034 smoke and dust plumes as a source of Na⁺ and (v) quantifying Cl⁻ depletion absolutely instead of
1035 relatively. Our finding that depletion reactions are extensive enough to alter rates of VOC
1036 oxidation along the USEC in May is impactful on multiple levels ranging from human health to
1037 regional radiative forcing, while reporting that inorganic acidic species are not contributing to
1038 these losses informs future works and the chemical modeling community that additional acidic
1039 species are critical to first identify and then to monitor. Finally, this study reveals the limitations
1040 in using traditional methods when quantifying Cl⁻ depletion and will hopefully motivate future
1041 works to either be mindful of these limitations or choose alternative methods.

1042 **Data availability**

1043 The ACTIVATE dataset can be found at
1044 <https://doi.org/10.5067/SUBORBITAL/ACTIVATE/DATA001> (ACTIVATE Science Team,
1045 2020). Level-3 (8-day, 4 km resolution) sea surface chlorophyll a concentrations from MODIS-
1046 Aqua can be found at <https://doi.org/10.5067/AQUA/MODIS/L3M/CHL/2022>.

1047 **Author contributions**

1048 YC, ECC, JPD, GSD, CER, MAS, ELW, and LDZ collected and/or prepared the data. ELE
1049 conducted the data analysis. ELE, ECC, and AS conducted data interpretation. ELE and AS
1050 prepared the manuscript with editing from [YC](#), ECC, JPD, GSD, MAS, ELW, and LDZ.

1051 **Competing interests**

1052 At least one of the (co-)authors is a member of the editorial board of Atmospheric Chemistry and
1053 Physics.

1054 **Disclaimer**

1055 Publisher's note: Copernicus Publications remains neutral with regard to jurisdictional claims in
1056 published maps and institutional affiliations.

1057

1058 **Acknowledgements**

1059 The authors acknowledge Claire Robinson for her contributions to this study and dedicate this to
1060 her. We thank pilots and aircraft maintenance personnel of NASA Langley Research Services
1061 Directorate for successfully conducting ACTIVATE flights and all others who were involved in
1062 executing the ACTIVATE campaign.

1063 **Financial support**

1064 This work was funded by ACTIVATE, a NASA Earth Venture Suborbital-3 (EVS-3) investigation
1065 funded by NASA's Earth Science Division and managed through the Earth System Science
1066 Pathfinder Program Office. University of Arizona investigators were funded by NASA grant no.
1067 80NSSC19K0442 and ONR grant no. N00014-21-1-2115.

1068 **References**

- 1069 ACTIVATE Science Team: Aerosol Cloud meTeorology Interactions oVer the western ATlantic
1070 Experiment Data, <https://doi.org/10.5067/SUBORBITAL/ACTIVATE/DATA001>, 2020.
- 1071 Adachi, K., Dibb, J. E., Scheuer, E., Katich, J. M., Schwarz, J. P., Perring, A. E., Mediavilla, B.,
1072 Guo, H., Campuzano-Jost, P., Jimenez, J. L., Crawford, J., Soja, A. J., Oshima, N., Kajino, M.,
1073 Kinase, T., Kleinman, L., Sedlacek III, A. J., Yokelson, R. J., and Buseck, P. R.: Fine Ash-
1074 Bearing Particles as a Major Aerosol Component in Biomass Burning Smoke, *Journal of*
1075 *Geophysical Research: Atmospheres*, 127, e2021JD035657,
1076 <https://doi.org/10.1029/2021JD035657>, 2022.
- 1077 Akagi, S. K., Yokelson, R. J., Burling, I. R., Meinardi, S., Simpson, I., Blake, D. R.,
1078 McMeeking, G. R., Sullivan, A., Lee, T., Kreidenweis, S., Urbanski, S., Reardon, J., Griffith, D.
1079 W. T., Johnson, T. J., and Weise, D. R.: Measurements of reactive trace gases and variable O₃
1080 formation rates in some South Carolina biomass burning plumes, *Atmospheric Chemistry and*
1081 *Physics*, 13, 1141–1165, <https://doi.org/10.5194/acp-13-1141-2013>, 2013.
- 1082 Aldhaif, A. M., Lopez, D. H., Dadashazar, H., and Sorooshian, A.: Sources, frequency, and
1083 chemical nature of dust events impacting the United States East Coast, *Atmospheric*
1084 *Environment*, 231, 117456, <https://doi.org/10.1016/j.atmosenv.2020.117456>, 2020.
- 1085 Al-Hosney, H. A., Carlos-Cuellar, S., Baltrusaitis, J., and Grassian, V. H.: Heterogeneous uptake
1086 and reactivity of formic acid on calcium carbonate particles: a Knudsen cell reactor, FTIR and
1087 SEM study, *Phys. Chem. Chem. Phys.*, 7, 3587–3595, <https://doi.org/10.1039/B510112C>, 2005.
- 1088 Andreae, M. O. and Merlet, P.: Emission of trace gases and aerosols from biomass burning,
1089 *Global Biogeochemical Cycles*, 15, 955–966, <https://doi.org/10.1029/2000GB001382>, 2001.
- 1090 Andreae, M. O., Andreae, T. W., Annegarn, H., Beer, J., Cachier, H., Le Canut, P., Elbert, W.,
1091 Maenhaut, W., Salma, I., Wienhold, F. G., and Zenker, T.: Airborne studies of aerosol emissions
1092 from savanna fires in southern Africa: 2. Aerosol chemical composition, *Journal of Geophysical*
1093 *Research: Atmospheres*, 103, 32119–32128, <https://doi.org/10.1029/98JD02280>, 1998.
- 1094 Andreae, M. O., Andreae, T. W., Meyerdierks, D., and Thiel, C.: Marine sulfur cycling and the
1095 atmospheric aerosol over the springtime North Atlantic, *Chemosphere*, 52, 1321–1343,
1096 [https://doi.org/10.1016/S0045-6535\(03\)00366-7](https://doi.org/10.1016/S0045-6535(03)00366-7), 2003.
- 1097 AzadiAghdam, M., Braun, R. A., Edwards, E.-L., Bañaga, P. A., Cruz, M. T., Betito, G.,
1098 Cambaliza, M. O., Dadashazar, H., Lorenzo, G. R., Ma, L., MacDonald, A. B., Nguyen, P.,
1099 Simpas, J. B., Stahl, C., and Sorooshian, A.: On the nature of sea salt aerosol at a coastal
1100 megacity: Insights from Manila, Philippines in Southeast Asia, *Atmospheric Environment*, 216,
1101 116922, <https://doi.org/10.1016/j.atmosenv.2019.116922>, 2019.
- 1102 Bondy, A. L., Wang, B., Laskin, A., Craig, R. L., Nhliziyo, M. V., Bertman, S. B., Pratt, K. A.,
1103 Shepson, P. B., and Ault, A. P.: Inland Sea Spray Aerosol Transport and Incomplete Chloride
1104 Depletion: Varying Degrees of Reactive Processing Observed during SOAS, *Environ. Sci.*
1105 *Technol.*, 51, 9533–9542, <https://doi.org/10.1021/acs.est.7b02085>, 2017.

- 1106 Boreddy, S. K. R. and Kawamura, K.: A 12-year observation of water-soluble ions in TSP
1107 aerosols collected at a remote marine location in the western North Pacific: an outflow region of
1108 Asian dust, *Atmospheric Chemistry and Physics*, 15, 6437–6453, [https://doi.org/10.5194/acp-15-](https://doi.org/10.5194/acp-15-6437-2015)
1109 [6437-2015](https://doi.org/10.5194/acp-15-6437-2015), 2015.
- 1110 Bowen, H. J. M.: *Environmental chemistry of the elements*, Academic Press, London, New
1111 York, xv, 333 pp., 1979.
- 1112 Braun, R. A., Dadashazar, H., MacDonald, A. B., Aldhaif, A. M., Maudlin, L. C., Crosbie, E.,
1113 Aghdam, M. A., Hossein Mardi, A., and Sorooshian, A.: Impact of Wildfire Emissions on
1114 Chloride and Bromide Depletion in Marine Aerosol Particles, *Environ. Sci. Technol.*, 51, 9013–
1115 9021, <https://doi.org/10.1021/acs.est.7b02039>, 2017.
- 1116 Braun, R. A., McComiskey, A., Tselioudis, G., Tropsch, D., and Sorooshian, A.: Cloud, Aerosol,
1117 and Radiative Properties Over the Western North Atlantic Ocean, *Journal of Geophysical*
1118 *Research: Atmospheres*, 126, e2020JD034113, <https://doi.org/10.1029/2020JD034113>, 2021.
- 1119 Buchholz, R. R., Worden, H. M., Park, M., Francis, G., Deeter, M. N., Edwards, D. P., Emmons,
1120 L. K., Gaubert, B., Gille, J., Martínez-Alonso, S., Tang, W., Kumar, R., Drummond, J. R.,
1121 Clerbaux, C., George, M., Coheur, P.-F., Hurtmans, D., Bowman, K. W., Luo, M., Payne, V. H.,
1122 Worden, J. R., Chin, M., Levy, R. C., Warner, J., Wei, Z., and Kulawik, S. S.: Air pollution
1123 trends measured from Terra: CO and AOD over industrial, fire-prone, and background regions,
1124 *Remote Sensing of Environment*, 256, 112275, <https://doi.org/10.1016/j.rse.2020.112275>, 2021.
- 1125 Cao, F., Zhang, S.-C., Kawamura, K., and Zhang, Y.-L.: Inorganic markers, carbonaceous
1126 components and stable carbon isotope from biomass burning aerosols in Northeast China,
1127 *Science of The Total Environment*, 572, 1244–1251,
1128 <https://doi.org/10.1016/j.scitotenv.2015.09.099>, 2016.
- 1129 Carlos-Cuellar, S., Li, P., Christensen, A. P., Krueger, B. J., Burrichter, C., and Grassian, V. H.:
1130 Heterogeneous Uptake Kinetics of Volatile Organic Compounds on Oxide Surfaces Using a
1131 Knudsen Cell Reactor: Adsorption of Acetic Acid, Formaldehyde, and Methanol on α -Fe₂O₃, α -
1132 Al₂O₃, and SiO₂, *J. Phys. Chem. A*, 107, 4250–4261, <https://doi.org/10.1021/jp0267609>, 2003.
- 1133 Chameides, W. L. and Stelson, A. W.: Reply [to “Comment on ‘Aqueous phase chemical
1134 processes in deliquescent sea-salt aerosols: A mechanism that couples the atmospheric cycles of
1135 S and sea salt’ by W. L. Chameides and A. W. Stelson”], *Journal of Geophysical Research:*
1136 *Atmospheres*, 98, 9051–9054, <https://doi.org/10.1029/93JD00310>, 1993.
- 1137 Chatterjee, A., Dutta, M., Ghosh, A., Ghosh, S. K., and Roy, A.: Relative role of black carbon
1138 and sea-salt aerosols as cloud condensation nuclei over a high altitude urban atmosphere in
1139 eastern Himalaya, *Science of The Total Environment*, 742, 140468,
1140 <https://doi.org/10.1016/j.scitotenv.2020.140468>, 2020.
- 1141 Chen, Z., Liu, P., Liu, Y., and Zhang, Y.-H.: Strong Acids or Bases Displaced by Weak Acids or
1142 Bases in Aerosols: Reactions Driven by the Continuous Partitioning of Volatile Products into the
1143 Gas Phase, *Acc. Chem. Res.*, 54, 3667–3678, <https://doi.org/10.1021/acs.accounts.1c00318>,
1144 2021.

- 1145 Cooper, O. R., Moody, J. L., Parrish, D. D., Trainer, M., Ryerson, T. B., Holloway, J. S., Hübler,
 1146 G., Fehsenfeld, F. C., Oltmans, S. J., and Evans, M. J.: Trace gas signatures of the airstreams
 1147 within North Atlantic cyclones: Case studies from the North Atlantic Regional Experiment
 1148 (NARE '97) aircraft intensive, *Journal of Geophysical Research: Atmospheres*, 106, 5437–5456,
 1149 <https://doi.org/10.1029/2000JD900574>, 2001.
- 1150 Cooper, O. R., Moody, J. L., Parrish, D. D., Trainer, M., Holloway, J. S., Hübler, G., Fehsenfeld,
 1151 F. C., and Stohl, A.: Trace gas composition of midlatitude cyclones over the western North
 1152 Atlantic Ocean: A seasonal comparison of O₃ and CO, *Journal of Geophysical Research:*
 1153 *Atmospheres*, 107, ACH 2-1-ACH 2-12, <https://doi.org/10.1029/2001JD000902>, 2002.
- 1154 Corral, A. F., Braun, R. A., Cairns, B., Gorooh, V. A., Liu, H., Ma, L., Mardi, A. H., Painemal,
 1155 D., Stamnes, S., van Dierenhoven, B., Wang, H., Yang, Y., Zhang, B., and Sorooshian, A.: An
 1156 Overview of Atmospheric Features Over the Western North Atlantic Ocean and North American
 1157 East Coast – Part 1: Analysis of Aerosols, Gases, and Wet Deposition Chemistry, *Journal of*
 1158 *Geophysical Research: Atmospheres*, 126, e2020JD032592,
 1159 <https://doi.org/10.1029/2020JD032592>, 2021.
- 1160 Corral, A. F., Choi, Y., Collister, B. L., Crosbie, E., Dadashazar, H., DiGangi, J. P., Diskin, G.
 1161 S., Fenn, M., Kirschler, S., Moore, R. H., Nowak, J. B., Shook, M. A., Stahl, C. T., Shingler, T.,
 1162 Thornhill, K. L., Voigt, C., Ziemba, L. D., and Sorooshian, A.: Dimethylamine in cloud water: a
 1163 case study over the northwest Atlantic Ocean, *Environ. Sci.: Atmos.*, 2, 1534–1550,
 1164 <https://doi.org/10.1039/D2EA00117A>, 2022.
- 1165 Crosbie, E., Shook, M. A., Ziemba, L. D., Anderson, B. E., Braun, R. A., Brown, M. D., Jordan,
 1166 C. E., MacDonald, A. B., Moore, R. H., Nowak, J. B., Robinson, C. E., Shingler, T., Sorooshian,
 1167 A., Stahl, C., Thornhill, K. L., Wiggins, E. B., and Winstead, E.: Coupling an online ion
 1168 conductivity measurement with the particle-into-liquid sampler: Evaluation and modeling using
 1169 laboratory and field aerosol data, *Aerosol Science and Technology*, 54, 1542–1555,
 1170 <https://doi.org/10.1080/02786826.2020.1795499>, 2020.
- 1171 Crosbie, E., Ziemba, L. D., Shook, M. A., Robinson, C. E., Winstead, E. L., Thornhill, K. L.,
 1172 Braun, R. A., MacDonald, A. B., Stahl, C., Sorooshian, A., van den Heever, S. C., DiGangi, J.
 1173 P., Diskin, G. S., Woods, S., Bañaga, P., Brown, M. D., Gallo, F., Hilario, M. R. A., Jordan, C.
 1174 E., Leung, G. R., Moore, R. H., Sanchez, K. J., Shingler, T. J., and Wiggins, E. B.: Measurement
 1175 report: Closure analysis of aerosol–cloud composition in tropical maritime warm convection,
 1176 *Atmospheric Chemistry and Physics*, 22, 13269–13302, [https://doi.org/10.5194/acp-22-13269-](https://doi.org/10.5194/acp-22-13269-2022)
 1177 2022, 2022.
- 1178 Cruz, M. T., Bañaga, P. A., Betito, G., Braun, R. A., Stahl, C., Aghdam, M. A., Cambaliza, M.
 1179 O., Dadashazar, H., Hilario, M. R., Lorenzo, G. R., Ma, L., MacDonald, A. B., Pabroa, P. C.,
 1180 Yee, J. R., Simpas, J. B., and Sorooshian, A.: Size-resolved composition and morphology of
 1181 particulate matter during the southwest monsoon in Metro Manila, Philippines, *Atmospheric*
 1182 *Chemistry and Physics*, 19, 10675–10696, [https://doi.org/10.5194/acp-19-10675-](https://doi.org/10.5194/acp-19-10675-2019)
 2019, 2019.
- 1183 Dadashazar, H., Alipanah, M., Hilario, M. R. A., Crosbie, E., Kirschler, S., Liu, H., Moore, R.
 1184 H., Peters, A. J., Scarino, A. J., Shook, M., Thornhill, K. L., Voigt, C., Wang, H., Winstead, E.,

- 1185 Zhang, B., Ziemba, L., and Sorooshian, A.: Aerosol responses to precipitation along North
 1186 American air trajectories arriving at Bermuda, *Atmospheric Chemistry and Physics*, 21, 16121–
 1187 16141, <https://doi.org/10.5194/acp-21-16121-2021>, 2021.
- 1188 Dang, C., Segal-Rozenhaimer, M., Che, H., Zhang, L., Formenti, P., Taylor, J., Dobracki, A.,
 1189 Purdue, S., Wong, P.-S., Nenes, A., Sedlacek III, A., Coe, H., Redemann, J., Zuidema, P.,
 1190 Howell, S., and Haywood, J.: Biomass burning and marine aerosol processing over the southeast
 1191 Atlantic Ocean: a TEM single-particle analysis, *Atmospheric Chemistry and Physics*, 22, 9389–
 1192 9412, <https://doi.org/10.5194/acp-22-9389-2022>, 2022.
- 1193 Davis, R. E., Hayden, B. P., Gay, D. A., Phillips, W. L., and Jones, G. V.: The North Atlantic
 1194 Subtropical Anticyclone, *Journal of Climate*, 10, 728–744, [https://doi.org/10.1175/1520-0442\(1997\)010<0728:TNASA>2.0.CO;2](https://doi.org/10.1175/1520-0442(1997)010<0728:TNASA>2.0.CO;2), 1997.
- 1196 DeCarlo, P. F., Dunlea, E. J., Kimmel, J. R., Aiken, A. C., Sueper, D., Crouse, J., Wennberg, P.
 1197 O., Emmons, L., Shinozuka, Y., Clarke, A., Zhou, J., Tomlinson, J., Collins, D. R., Knapp, D.,
 1198 Weinheimer, A. J., Montzka, D. D., Campos, T., and Jimenez, J. L.: Fast airborne aerosol size
 1199 and chemistry measurements above Mexico City and Central Mexico during the MILAGRO
 1200 campaign, *Atmospheric Chemistry and Physics*, 8, 4027–4048, <https://doi.org/10.5194/acp-8-4027-2008>, 2008.
- 1202 DiGangi, J. P., Choi, Y., Nowak, J. B., Halliday, H. S., Diskin, G. S., Feng, S., Barkley, Z. R.,
 1203 Lauvaux, T., Pal, S., Davis, K. J., Baier, B. C., and Sweeney, C.: Seasonal Variability in Local
 1204 Carbon Dioxide Biomass Burning Sources Over Central and Eastern US Using Airborne In Situ
 1205 Enhancement Ratios, *Journal of Geophysical Research: Atmospheres*, 126, e2020JD034525,
 1206 <https://doi.org/10.1029/2020JD034525>, 2021.
- 1207 Diskin, G. S., Podolske, J. R., Sachse, G. W., and Slate, T. A.: Open-path airborne tunable diode
 1208 laser hygrometer, in: *Diode Lasers and Applications in Atmospheric Sensing*, *Diode Lasers and*
 1209 *Applications in Atmospheric Sensing*, 196–204, <https://doi.org/10.1117/12.453736>, 2002.
- 1210 Drozd, G., Woo, J., Häkkinen, S. a. K., Nenes, A., and McNeill, V. F.: Inorganic salts interact
 1211 with oxalic acid in submicron particles to form material with low hygroscopicity and volatility,
 1212 *Atmospheric Chemistry and Physics*, 14, 5205–5215, <https://doi.org/10.5194/acp-14-5205-2014>,
 1213 2014.
- 1214 Echalar, F., Gaudichet, A., Cachier, H., and Artaxo, P.: Aerosol emissions by tropical forest and
 1215 savanna biomass burning: Characteristic trace elements and fluxes, *Geophysical Research*
 1216 *Letters*, 22, 3039–3042, <https://doi.org/10.1029/95GL03170>, 1995.
- 1217 Edwards, E.-L., Corral, A. F., Dadashazar, H., Barkley, A. E., Gaston, C. J., Zuidema, P., and
 1218 Sorooshian, A.: Impact of various air mass types on cloud condensation nuclei concentrations
 1219 along coastal southeast Florida, *Atmospheric Environment*, 254, 118371,
 1220 <https://doi.org/10.1016/j.atmosenv.2021.118371>, 2021.
- 1221 Eichler, T. and Higgins, W.: Climatology and ENSO-Related Variability of North American
 1222 Extratropical Cyclone Activity, *Journal of Climate*, 19, 2076–2093,
 1223 <https://doi.org/10.1175/JCLI3725.1>, 2006.

- 1224 Faxon, C. B. and Allen, D. T.: Chlorine chemistry in urban atmospheres: a review, *Environ.*
 1225 *Chem.*, 10, 221–233, <https://doi.org/10.1071/EN13026>, 2013.
- 1226 Fehsenfeld, F. C., Ancellet, G., Bates, T. S., Goldstein, A. H., Hardesty, R. M., Honrath, R.,
 1227 Law, K. S., Lewis, A. C., Leaitch, R., McKeen, S., Meagher, J., Parrish, D. D., Pszenny, A. A.
 1228 P., Russell, P. B., Schlager, H., Seinfeld, J., Talbot, R., and Zbinden, R.: International
 1229 Consortium for Atmospheric Research on Transport and Transformation (ICARTT): North
 1230 America to Europe—Overview of the 2004 summer field study, *Journal of Geophysical*
 1231 *Research (Atmospheres)*, 111, D23S01, <https://doi.org/10.1029/2006JD007829>, 2006.
- 1232 Feng, J., Chan, E., and Vet, R.: Air quality in the eastern United States and Eastern Canada for
 1233 1990–2015: 25 years of change in response to emission reductions of SO₂ and NO_x in the region,
 1234 *Atmospheric Chemistry and Physics*, 20, 3107–3134, <https://doi.org/10.5194/acp-20-3107-2020>,
 1235 2020.
- 1236 Feng, L., Shen, H., Zhu, Y., Gao, H., and Yao, X.: Insight into Generation and Evolution of Sea-
 1237 Salt Aerosols from Field Measurements in Diversified Marine and Coastal Atmospheres, *Sci*
 1238 *Rep.*, 7, 41260, <https://doi.org/10.1038/srep41260>, 2017.
- 1239 Ferrare, R., Hair, J., Hostetler, C., Shingler, T., Burton, S. P., Fenn, M., Clayton, M., Scarino, A.
 1240 J., Harper, D., Seaman, S., Cook, A., Crosbie, E., Winstead, E., Ziemba, L., Thornhill, L.,
 1241 Robinson, C., Moore, R., Vaughan, M., Sorooshian, A., Schlosser, J. S., Liu, H., Zhang, B.,
 1242 Diskin, G., DiGangi, J., Nowak, J., Choi, Y., Zuidema, P., and Chellappan, S.: Airborne HSRL-2
 1243 measurements of elevated aerosol depolarization associated with non-spherical sea salt, *Frontiers*
 1244 *in Remote Sensing*, 4, 01–18, <https://doi.org/10.3389/frsen.2023.1143944>, 2023.
- 1245 Finlayson-Pitts, B. J. and Pitts, J. N.: CHAPTER 9 - Particles in the Troposphere, in: *Chemistry*
 1246 *of the Upper and Lower Atmosphere*, edited by: Finlayson-Pitts, B. J. and Pitts, J. N., Academic
 1247 Press, San Diego, 349–435, <https://doi.org/10.1016/B978-012257060-5/50011-3>, 2000.
- 1248 Galloway, J. N., Savoie, D. L., Keene, W. C., and Prospero, J. M.: The temporal and spatial
 1249 variability of scavenging ratios for NSS sulfate, nitrate, methanesulfonate and sodium in the
 1250 Atmosphere over the North Atalantic Ocean, *Atmospheric Environment. Part A. General Topics*,
 1251 27, 235–250, [https://doi.org/10.1016/0960-1686\(93\)90354-2](https://doi.org/10.1016/0960-1686(93)90354-2), 1993.
- 1252 Gelaro, R., McCarty, W., Suárez, M. J., Todling, R., Molod, A., Takacs, L., Randles, C. A.,
 1253 Darmenov, A., Bosilovich, M. G., Reichle, R., Wargan, K., Coy, L., Cullather, R., Draper, C.,
 1254 Akella, S., Buchard, V., Conaty, A., Silva, A. M. da, Gu, W., Kim, G.-K., Koster, R., Lucchesi,
 1255 R., Merkova, D., Nielsen, J. E., Partyka, G., Pawson, S., Putman, W., Rienecker, M., Schubert,
 1256 S. D., Sienkiewicz, M., and Zhao, B.: The Modern-Era Retrospective Analysis for Research and
 1257 Applications, Version 2 (MERRA-2), *Journal of Climate*, 30, 5419–5454,
 1258 <https://doi.org/10.1175/JCLI-D-16-0758.1>, 2017.
- 1259 Ghorai, S., Wang, B., Tivanski, A., and Laskin, A.: Hygroscopic Properties of Internally Mixed
 1260 Particles Composed of NaCl and Water-Soluble Organic Acids, *Environ. Sci. Technol.*, 48,
 1261 2234–2241, <https://doi.org/10.1021/es404727u>, 2014.

1262 Grandey, B. S., Stier, P., Wagner, T. M., Grainger, R. G., and Hodges, K. I.: The effect of
1263 extratropical cyclones on satellite-retrieved aerosol properties over ocean, *Geophysical Research*
1264 *Letters*, 38, L13805, <https://doi.org/10.1029/2011GL047703>, 2011.

1265 Grassian, V. H.: Chemical Reactions of Nitrogen Oxides on the Surface of Oxide, Carbonate,
1266 Soot, and Mineral Dust Particles: Implications for the Chemical Balance of the Troposphere, *J.*
1267 *Phys. Chem. A*, 106, 860–877, <https://doi.org/10.1021/jp012139h>, 2002.

1268 Hanisch, F. and Crowley, J. N.: Heterogeneous reactivity of NO and HNO₃ on mineral dust in
1269 the presence of ozone, *Phys. Chem. Chem. Phys.*, 5, 883–887,
1270 <https://doi.org/10.1039/B211503D>, 2003.

1271 Haskins, J. D., Jaeglé, L., Shah, V., Lee, B. H., Lopez-Hilfiker, F. D., Campuzano-Jost, P.,
1272 Schroder, J. C., Day, D. A., Guo, H., Sullivan, A. P., Weber, R., Dibb, J., Campos, T., Jimenez,
1273 J. L., Brown, S. S., and Thornton, J. A.: Wintertime Gas-Particle Partitioning and Speciation of
1274 Inorganic Chlorine in the Lower Troposphere Over the Northeast United States and Coastal
1275 Ocean, *Journal of Geophysical Research: Atmospheres*, 123, 12,897-12,916,
1276 <https://doi.org/10.1029/2018JD028786>, 2018.

1277 Hawcroft, M. K., Shaffrey, L. C., Hodges, K. I., and Dacre, H. F.: How much Northern
1278 Hemisphere precipitation is associated with extratropical cyclones?, *Geophysical Research*
1279 *Letters*, 39, L24809, <https://doi.org/10.1029/2012GL053866>, 2012.

1280 Hilario, M. R. A., Crosbie, E., Bañaga, P. A., Betito, G., Braun, R. A., Cambaliza, M. O., Corral,
1281 A. F., Cruz, M. T., Dibb, J. E., Lorenzo, G. R., MacDonald, A. B., Robinson, C. E., Shook, M.
1282 A., Simpas, J. B., Stahl, C., Winstead, E., Ziemba, L. D., and Sorooshian, A.: Particulate
1283 Oxalate-To-Sulfate Ratio as an Aqueous Processing Marker: Similarity Across Field Campaigns
1284 and Limitations, *Geophysical Research Letters*, 48, e2021GL096520,
1285 <https://doi.org/10.1029/2021GL096520>, 2021.

1286 Hogan, T. F., Liu, M., Ridout, J. A., Peng, M. S., Whitcomb, T. R., Ruston, B. C., Reynolds, C.
1287 A., Eckermann, S. D., Moskaitis, J. R., Baker, N. L., McCORMACK, J. P., Viner, K. C.,
1288 McLAY, J. G., Flatau, M. K., Xu, L., Chen, C., and Chang, S. W.: The Navy Global
1289 Environmental Model, *Oceanography*, 27, 116–125, <https://doi.org/10.5670/oceanog.2014.73>,
1290 2014.

1291 Huang, X., Olmez, I., Aras, N. K., and Gordon, G. E.: Emissions of trace elements from motor
1292 vehicles: Potential marker elements and source composition profile, *Atmospheric Environment*,
1293 28, 1385–1391, [https://doi.org/10.1016/1352-2310\(94\)90201-1](https://doi.org/10.1016/1352-2310(94)90201-1), 1994.

1294 Hyer, E. J., Reid, J. S., Prins, E. M., Hoffman, J. P., Schmidt, C. C., Miettinen, J. I., and Giglio,
1295 L.: Patterns of fire activity over Indonesia and Malaysia from polar and geostationary satellite
1296 observations, *Atmospheric Research*, 122, 504–519,
1297 <https://doi.org/10.1016/j.atmosres.2012.06.011>, 2013.

1298 J. S. Reid, E. J. Hyer, E. M. Prins, D. L. Westphal, J. Zhang, J. Wang, S. A. Christopher, C. A.
1299 Curtis, C. C. Schmidt, D. P. Eleuterio, K. A. Richardson, and J. P. Hoffman: Global Monitoring
1300 and Forecasting of Biomass-Burning Smoke: Description of and Lessons From the Fire Locating

- 1301 and Modeling of Burning Emissions (FLAMBE) Program, *IEEE Journal of Selected Topics in*
 1302 *Applied Earth Observations and Remote Sensing*, 2, 144–162,
 1303 <https://doi.org/10.1109/JSTARS.2009.2027443>, 2009.
- 1304 Jaffe, D. A., O’Neill, S. M., Larkin, N. K., Holder, A. L., Peterson, D. L., Halofsky, J. E., and
 1305 Rappold, A. G.: Wildfire and prescribed burning impacts on air quality in the United States,
 1306 *Journal of the Air & Waste Management Association*, 70, 583–615,
 1307 <https://doi.org/10.1080/10962247.2020.1749731>, 2020.
- 1308 Jing, B., Peng, C., Wang, Y., Liu, Q., Tong, S., Zhang, Y., and Ge, M.: Hygroscopic properties
 1309 of potassium chloride and its internal mixtures with organic compounds relevant to biomass
 1310 burning aerosol particles, *Sci Rep*, 7, 43572, <https://doi.org/10.1038/srep43572>, 2017.
- 1311 Kacenenbogen, M. S. F., Tan, Q., Burton, S. P., Hasekamp, O. P., Froyd, K. D., Shinozuka, Y.,
 1312 Beyersdorf, A. J., Ziemba, L., Thornhill, K. L., Dibb, J. E., Shingler, T., Sorooshian, A.,
 1313 Espinosa, R. W., Martins, V., Jimenez, J. L., Campuzano-Jost, P., Schwarz, J. P., Johnson, M. S.,
 1314 Redemann, J., and Schuster, G. L.: Identifying chemical aerosol signatures using optical
 1315 suborbital observations: how much can optical properties tell us about aerosol composition?,
 1316 *Atmospheric Chemistry and Physics*, 22, 3713–3742, <https://doi.org/10.5194/acp-22-3713-2022>,
 1317 2022.
- 1318 Kavouras, I. G., Nikolich, G., Etyemezian, V., DuBois, D. W., King, J., and Shafer, D.: In situ
 1319 observations of soil minerals and organic matter in the early phases of prescribed fires, *Journal of*
 1320 *Geophysical Research: Atmospheres*, 117, D12313, <https://doi.org/10.1029/2011JD017420>,
 1321 2012.
- 1322 Keene, W. C. and Savoie, D. L.: The pH of deliquesced sea-salt aerosol in polluted marine air,
 1323 *Geophysical Research Letters*, 25, 2181–2184, <https://doi.org/10.1029/98GL01591>, 1998.
- 1324 Keene, W. C., Pszenny, A. A. P., Jacob, D. J., Duce, R. A., Galloway, J. N., Schultz-Tokos, J. J.,
 1325 Sievering, H., and Boatman, J. F.: The geochemical cycling of reactive chlorine through the
 1326 marine troposphere, *Global Biogeochemical Cycles*, 4, 407–430,
 1327 <https://doi.org/10.1029/GB004i004p00407>, 1990.
- 1328 Keene, W. C., Pszenny, A. A. P., Maben, J. R., Stevenson, E., and Wall, A.: Closure evaluation
 1329 of size-resolved aerosol pH in the New England coastal atmosphere during summer, *Journal of*
 1330 *Geophysical Research: Atmospheres*, 109, D23307, <https://doi.org/10.1029/2004JD004801>,
 1331 2004.
- 1332 Keene, W. C., Stutz, J., Pszenny, A. A. P., Maben, J. R., Fischer, E. V., Smith, A. M., von
 1333 Glasow, R., Pechtl, S., Sive, B. C., and Varner, R. K.: Inorganic chlorine and bromine in coastal
 1334 New England air during summer, *Journal of Geophysical Research: Atmospheres*, 112, D10S12,
 1335 <https://doi.org/10.1029/2006JD007689>, 2007.
- 1336 Keene, William. C., Khalil, M. A. K., Erickson III, David. J., McCulloch, A., Graedel, T. E.,
 1337 Lobert, J. M., Aucott, M. L., Gong, S. L., Harper, D. B., Kleiman, G., Midgley, P., Moore, R.
 1338 M., Seuzaret, C., Sturges, W. T., Benkovitz, C. M., Koropalov, V., Barrie, L. A., and Li, Y. F.:
 1339 Composite global emissions of reactive chlorine from anthropogenic and natural sources:

- 1340 Reactive Chlorine Emissions Inventory, *Journal of Geophysical Research: Atmospheres*, 104,
1341 8429–8440, <https://doi.org/10.1029/1998JD100084>, 1999.
- 1342 Keim, B. D., Meeker, L. D., and Slater, J. F.: Manual synoptic climate classification for the east
1343 coast of New England (USA) with an application to PM_{2.5} concentration, *Climate Research*, 28,
1344 143–153, <https://doi.org/10.3354/cr028143>, 2005.
- 1345 Kerminen, V.-M., Teinilä, K., Hillamo, R., and Pakkanen, T.: Substitution of chloride in sea-salt
1346 particles by inorganic and organic anions, *Journal of Aerosol Science*, 29, 929–942,
1347 [https://doi.org/10.1016/S0021-8502\(98\)00002-0](https://doi.org/10.1016/S0021-8502(98)00002-0), 1998.
- 1348 Knipping, E. M. and Dabdub, D.: Impact of Chlorine Emissions from Sea-Salt Aerosol on
1349 Coastal Urban Ozone, *Environ. Sci. Technol.*, 37, 275–284, <https://doi.org/10.1021/es025793z>,
1350 2003.
- 1351 Kong, S., Wen, B., Chen, K., Yin, Y., Li, L., Li, Q., Yuan, L., Li, X., and Sun, X.: Ion chemistry
1352 for atmospheric size-segregated aerosol and depositions at an offshore site of Yangtze River
1353 Delta region, China, *Atmospheric Research*, 147–148, 205–226,
1354 <https://doi.org/10.1016/j.atmosres.2014.05.018>, 2014.
- 1355 Kuklinska, K., Wolska, L., and Namiesnik, J.: Air quality policy in the U.S. and the EU – a
1356 review, *Atmospheric Pollution Research*, 6, 129–137, <https://doi.org/10.5094/APR.2015.015>,
1357 2015.
- 1358 Lamberg, H., Nuutinen, K., Tissari, J., Ruusunen, J., Yli-Pirilä, P., Sippula, O., Tapanainen, M.,
1359 Jalava, P., Makkonen, U., Teinilä, K., Saarnio, K., Hillamo, R., Hirvonen, M.-R., and Jokiniemi,
1360 J.: Physicochemical characterization of fine particles from small-scale wood combustion,
1361 *Atmospheric Environment*, 45, 7635–7643, <https://doi.org/10.1016/j.atmosenv.2011.02.072>,
1362 2011.
- 1363 Laskin, A., Moffet, R. C., Gilles, M. K., Fast, J. D., Zaveri, R. A., Wang, B., Nigge, P., and
1364 Shutthanandan, J.: Tropospheric chemistry of internally mixed sea salt and organic particles:
1365 Surprising reactivity of NaCl with weak organic acids, *Journal of Geophysical Research:*
1366 *Atmospheres*, 117, D15302, <https://doi.org/10.1029/2012JD017743>, 2012.
- 1367 Li, J., Pósfai, M., Hobbs, P. V., and Buseck, P. R.: Individual aerosol particles from biomass
1368 burning in southern Africa: 2, Compositions and aging of inorganic particles, *Journal of*
1369 *Geophysical Research: Atmospheres*, 108, 8484, <https://doi.org/10.1029/2002JD002310>, 2003.
- 1370 Lippmann, M.: HEALTH EFFECTS OF OZONE A Critical Review, *JAPCA*, 39, 672–695,
1371 <https://doi.org/10.1080/08940630.1989.10466554>, 1989.
- 1372 Luria, M., Van Valin, C. C., Galloway, J. N., Keene, W. C., Wellman, D. L., Sievering, H., and
1373 Boatman, J. F.: The relationship between dimethyl sulfide and particulate sulfate in the mid-
1374 atlantic ocean atmosphere, *Atmospheric Environment*, 23, 139–147,
1375 [https://doi.org/10.1016/0004-6981\(89\)90106-6](https://doi.org/10.1016/0004-6981(89)90106-6), 1989.

- 1376 Lynch, P., Reid, J. S., Westphal, D. L., Zhang, J., Hogan, T. F., Hyer, E. J., Curtis, C. A., Hegg,
1377 D. A., Shi, Y., Campbell, J. R., Rubin, J. I., Sessions, W. R., Turk, F. J., and Walker, A. L.: An
1378 11-year global gridded aerosol optical thickness reanalysis (v1.0) for atmospheric and climate
1379 sciences, *Geoscientific Model Development*, 9, 1489–1522, [https://doi.org/10.5194/gmd-9-1489-](https://doi.org/10.5194/gmd-9-1489-2016)
1380 2016, 2016.
- 1381 Mardi, A. H., Dadashazar, H., Painemal, D., Shingler, T., Seaman, S. T., Fenn, M. A., Hostetler,
1382 C. A., and Sorooshian, A.: Biomass Burning Over the United States East Coast and Western
1383 North Atlantic Ocean: Implications for Clouds and Air Quality, *Journal of Geophysical*
1384 *Research: Atmospheres*, 126, e2021JD034916, <https://doi.org/10.1029/2021JD034916>, 2021.
- 1385 Maudlin, L. C., Wang, Z., Jonsson, H. H., and Sorooshian, A.: Impact of wildfires on size-
1386 resolved aerosol composition at a coastal California site, *Atmospheric Environment*, 119, 59–68,
1387 <https://doi.org/10.1016/j.atmosenv.2015.08.039>, 2015.
- 1388 McCarty, J. L., Justice, C. O., and Korontzi, S.: Agricultural burning in the Southeastern United
1389 States detected by MODIS, *Remote Sensing of Environment*, 108, 151–162,
1390 <https://doi.org/10.1016/j.rse.2006.03.020>, 2007.
- 1391 McNaughton, C. S., Clarke, A. D., Howell, S. G., Pinkerton, M., Anderson, B., Thornhill, L.,
1392 Hudgins, C., Winstead, E., Dibb, J. E., Scheuer, E., and Maring, H.: Results from the DC-8 Inlet
1393 Characterization Experiment (DICE): Airborne Versus Surface Sampling of Mineral Dust and
1394 Sea Salt Aerosols, *Aerosol Science and Technology*, 41, 136–159,
1395 <https://doi.org/10.1080/02786820601118406>, 2007.
- 1396 Moffet, R. C., Desyaterik, Y., Hopkins, R. J., Tivanski, A. V., Gilles, M. K., Wang, Y.,
1397 Shutthanandan, V., Molina, L. T., Abraham, R. G., Johnson, K. S., Mugica, V., Molina, M. J.,
1398 Laskin, A., and Prather, K. A.: Characterization of aerosols containing Zn, Pb, and Cl from an
1399 industrial region of Mexico City, *Environ Sci Technol*, 42, 7091–7097,
1400 <https://doi.org/10.1021/es7030483>, 2008.
- 1401 Molina, M. J. and Rowland, F. S.: Stratospheric sink for chlorofluoromethanes: chlorine atom-
1402 catalysed destruction of ozone, *Nature*, 249, 810–812, <https://doi.org/10.1038/249810a0>, 1974.
- 1403 Naeher, L. P., Smith, K. R., Leaderer, B. P., Neufeld, L., and Mage, D. T.: Carbon Monoxide As
1404 a Tracer for Assessing Exposures to Particulate Matter in Wood and Gas Cookstove Households
1405 of Highland Guatemala, *Environ. Sci. Technol.*, 35, 575–581, <https://doi.org/10.1021/es991225g>,
1406 2001.
- 1407 Nolte, C., Bhave, P., Arnold, J., Dennis, R., Zhang, K., and Wexler, A.: Modeling urban and
1408 regional aerosols—Application of the CMAQ-UCD Aerosol Model to Tampa, a coastal urban
1409 site, *Atmospheric Environment*, 42, 3179–3191, <https://doi.org/10.1016/j.atmosenv.2007.12.059>,
1410 2008.
- 1411 Nuvolone, D., Petri, D., and Voller, F.: The effects of ozone on human health, *Environ Sci Pollut*
1412 *Res*, 25, 8074–8088, <https://doi.org/10.1007/s11356-017-9239-3>, 2018.

- 1413 Ondov, J. M., Choquette, C. E., Zoller, W. H., Gordon, G. E., Biermann, A. H., and Heft, R. E.:
 1414 Atmospheric behavior of trace elements on particles emitted from a coal-fired power plant,
 1415 *Atmospheric Environment*, 23, 2193–2204, [https://doi.org/10.1016/0004-6981\(89\)90181-9](https://doi.org/10.1016/0004-6981(89)90181-9),
 1416 1989.
- 1417 Ooki, A. and Uematsu, M.: Chemical interactions between mineral dust particles and acid gases
 1418 during Asian dust events, *Journal of Geophysical Research: Atmospheres*, 110,
 1419 <https://doi.org/10.1029/2004JD004737>, 2005.
- 1420 Ooki, A., Uematsu, M., Miura, K., and Nakae, S.: Sources of sodium in atmospheric fine
 1421 particles, *Atmospheric Environment*, 36, 4367–4374, [https://doi.org/10.1016/S1352-2310\(02\)00341-2](https://doi.org/10.1016/S1352-2310(02)00341-2), 2002.
- 1423 Osthoff, H. D., Roberts, J. M., Ravishankara, A. R., Williams, E. J., Lerner, B. M., Sommariva,
 1424 R., Bates, T. S., Coffman, D., Quinn, P. K., Dibb, J. E., Stark, H., Burkholder, J. B., Talukdar, R.
 1425 K., Meagher, J., Fehsenfeld, F. C., and Brown, S. S.: High levels of nitryl chloride in the polluted
 1426 subtropical marine boundary layer, *Nature Geoscience*, 1, 324–328,
 1427 <https://doi.org/10.1038/ngeo177>, 2008.
- 1428 Painemal, D., Corral, A. F., Sorooshian, A., Brunke, M. A., Chellappan, S., Afzali Gorooh, V.,
 1429 Ham, S.-H., O’Neill, L., Smith Jr., W. L., Tselioudis, G., Wang, H., Zeng, X., and Zuidema, P.:
 1430 An Overview of Atmospheric Features Over the Western North Atlantic Ocean and North
 1431 American East Coast—Part 2: Circulation, Boundary Layer, and Clouds, *Journal of Geophysical*
 1432 *Research: Atmospheres*, 126, e2020JD033423, <https://doi.org/10.1029/2020JD033423>, 2021.
- 1433 Palmer, T. Y.: Large fire winds, gases and smoke, *Atmospheric Environment*, 15, 2079–2090,
 1434 [https://doi.org/10.1016/0004-6981\(81\)90241-9](https://doi.org/10.1016/0004-6981(81)90241-9), 1981.
- 1435 Panagi, M., Fleming, Z. L., Monks, P. S., Ashfold, M. J., Wild, O., Hollaway, M., Zhang, Q.,
 1436 Squires, F. A., and Vande Hey, J. D.: Investigating the regional contributions to air pollution in
 1437 Beijing: a dispersion modelling study using CO as a tracer, *Atmospheric Chemistry and Physics*,
 1438 20, 2825–2838, <https://doi.org/10.5194/acp-20-2825-2020>, 2020.
- 1439 Park, S.-S., Sim, S. Y., Bae, M.-S., and Schauer, J. J.: Size distribution of water-soluble
 1440 components in particulate matter emitted from biomass burning, *Atmospheric Environment*, 73,
 1441 62–72, <https://doi.org/10.1016/j.atmosenv.2013.03.025>, 2013.
- 1442 Parungo, F. P., Nagamoto, C. T., Madel, R., Rosinski, J., and Haagenson, P. L.: Marine aerosols
 1443 in pacific upwelling regions, *Journal of Aerosol Science*, 18, 277–290,
 1444 [https://doi.org/10.1016/0021-8502\(87\)90023-1](https://doi.org/10.1016/0021-8502(87)90023-1), 1987.
- 1445 Pechtl, S. and von Glasow, R.: Reactive chlorine in the marine boundary layer in the outflow of
 1446 polluted continental air: A model study, *Geophysical Research Letters*, 34, L11813,
 1447 <https://doi.org/10.1029/2007GL029761>, 2007.
- 1448 Perry, K. D., Cahill, T. A., Eldred, R. A., Dutcher, D. D., and Gill, T. E.: Long-range transport of
 1449 North African dust to the eastern United States, *Journal of Geophysical Research: Atmospheres*,
 1450 102, 11225–11238, <https://doi.org/10.1029/97JD00260>, 1997.

- 1451 Popovicheva, O., Kistler, M., Kireeva, E., Persiantseva, N., Timofeev, M., Kopeikin, V., and
1452 Kasper-Giebl, A.: Physicochemical characterization of smoke aerosol during large-scale
1453 wildfires: Extreme event of August 2010 in Moscow, *Atmospheric Environment*, 96, 405–414,
1454 <https://doi.org/10.1016/j.atmosenv.2014.03.026>, 2014.
- 1455 Prospero, J. M.: Saharan Dust Transport Over the North Atlantic Ocean and Mediterranean: An
1456 Overview, in: *The Impact of Desert Dust Across the Mediterranean*, edited by: Guerzoni, S. and
1457 Chester, R., Springer Netherlands, Dordrecht, 133–151, https://doi.org/10.1007/978-94-017-3354-0_13, 1996.
- 1459 Prospero, J. M.: Long-term measurements of the transport of African mineral dust to the
1460 southeastern United States: Implications for regional air quality, *Journal of Geophysical*
1461 *Research: Atmospheres*, 104, 15917–15927, <https://doi.org/10.1029/1999JD900072>, 1999.
- 1462 Quinn, P. K. and Bates, T. S.: Regional aerosol properties: Comparisons of boundary layer
1463 measurements from ACE 1, ACE 2, Aerosols99, INDOEX, ACE Asia, TARFOX, and NEAQS,
1464 *Journal of Geophysical Research: Atmospheres*, 110, D14202,
1465 <https://doi.org/10.1029/2004JD004755>, 2005.
- 1466 Randles, C. A., Russell, L. M., and Ramaswamy, V.: Hygroscopic and optical properties of
1467 organic sea salt aerosol and consequences for climate forcing, *Geophysical Research Letters*, 31,
1468 L16108, <https://doi.org/10.1029/2004GL020628>, 2004.
- 1469 Rastogi, N., Agnihotri, R., Sawlani, R., Patel, A., Babu, S. S., and Satish, R.: Chemical and
1470 isotopic characteristics of PM₁₀ over the Bay of Bengal: Effects of continental outflow on a
1471 marine environment, *Science of The Total Environment*, 726, 138438,
1472 <https://doi.org/10.1016/j.scitotenv.2020.138438>, 2020.
- 1473 Reid, J. S., Jonsson, H. H., Smith, M. H., and Smirnov, A.: Evolution of the vertical profile and
1474 flux of large sea-salt particles in a coastal zone, *Journal of Geophysical Research: Atmospheres*,
1475 106, 12039–12053, <https://doi.org/10.1029/2000JD900848>, 2001.
- 1476 Riedel, T. P., Wolfe, G. M., Danas, K. T., Gilman, J. B., Kuster, W. C., Bon, D. M., Vlasenko,
1477 A., Li, S.-M., Williams, E. J., Lerner, B. M., Veres, P. R., Roberts, J. M., Holloway, J. S., Lefer,
1478 B., Brown, S. S., and Thornton, J. A.: An MCM modeling study of nitryl chloride (ClNO₂)
1479 impacts on oxidation, ozone production and nitrogen oxide partitioning in polluted continental
1480 outflow, *Atmospheric Chemistry and Physics*, 14, 3789–3800, <https://doi.org/10.5194/acp-14-3789-2014>, 2014.
- 1482 Roberts, J. M., Osthoff, H. D., Brown, S. S., and Ravishankara, A. R.: N₂O₅ Oxidizes Chloride
1483 to Cl₂ in Acidic Atmospheric Aerosol, *Science*, 321, 1059–1059,
1484 <https://doi.org/10.1126/science.1158777>, 2008.
- 1485 Robinson, A. L., Donahue, N. M., Shrivastava, M. K., Weitkamp, E. A., Sage, A. M., Grieshop,
1486 A. P., Lane, T. E., Pierce, J. R., and Pandis, S. N.: Rethinking Organic Aerosols: Semivolatile
1487 Emissions and Photochemical Aging, *Science*, 315, 1259–1262,
1488 <https://doi.org/10.1126/science.1133061>, 2007.

- 1489 Saide, P. E., Carmichael, G. R., Spak, S. N., Gallardo, L., Osses, A. E., Mena-Carrasco, M. A.,
1490 and Pagowski, M.: Forecasting urban PM₁₀ and PM_{2.5} pollution episodes in very stable
1491 nocturnal conditions and complex terrain using WRF–Chem CO tracer model, *Atmospheric*
1492 *Environment*, 45, 2769–2780, <https://doi.org/10.1016/j.atmosenv.2011.02.001>, 2011.
- 1493 Santschi, Ch. and Rossi, M. J.: Uptake of CO₂, SO₂, HNO₃ and HCl on Calcite (CaCO₃) at 300
1494 K: Mechanism and the Role of Adsorbed Water, *J. Phys. Chem. A*, 110, 6789–6802,
1495 <https://doi.org/10.1021/jp056312b>, 2006.
- 1496 Savoie, D. L., Arimoto, R., Keene, W. C., Prospero, J. M., Duce, R. A., and Galloway, J. N.:
1497 Marine biogenic and anthropogenic contributions to non-sea-salt sulfate in the marine boundary
1498 layer over the North Atlantic Ocean, *Journal of Geophysical Research: Atmospheres*, 107, AAC
1499 3-1-AAC 3-21, <https://doi.org/10.1029/2001JD000970>, 2002.
- 1500 Schlosser, J. S., Braun, R. A., Bradley, T., Dadashazar, H., MacDonald, A. B., Aldhaif, A. A.,
1501 Aghdam, M. A., Mardi, A. H., Xian, P., and Sorooshian, A.: Analysis of aerosol composition
1502 data for western United States wildfires between 2005 and 2015: Dust emissions, chloride
1503 depletion, and most enhanced aerosol constituents, *Journal of Geophysical Research:*
1504 *Atmospheres*, 122, 8951–8966, <https://doi.org/10.1002/2017JD026547>, 2017.
- 1505 Schroder, J. C., Campuzano-Jost, P., Day, D. A., Shah, V., Larson, K., Sommers, J. M., Sullivan,
1506 A. P., Campos, T., Reeves, J. M., Hills, A., Hornbrook, R. S., Blake, N. J., Scheuer, E., Guo, H.,
1507 Fibiger, D. L., McDuffie, E. E., Hayes, P. L., Weber, R. J., Dibb, J. E., Apel, E. C., Jaeglé, L.,
1508 Brown, S. S., Thornton, J. A., and Jimenez, J. L.: Sources and Secondary Production of Organic
1509 Aerosols in the Northeastern United States during WINTER, *Journal of Geophysical Research:*
1510 *Atmospheres*, 123, 7771–7796, <https://doi.org/10.1029/2018JD028475>, 2018.
- 1511 Seinfeld, J. H. and Pandis, S. N.: *Atmospheric Chemistry and Physics: From Air Pollution to*
1512 *Climate Change*, John Wiley & Sons, 1146 pp., 2016.
- 1513 Shingler, T., Dey, S., Sorooshian, A., Brechtel, F. J., Wang, Z., Metcalf, A., Coggon, M.,
1514 Mülmenstädt, J., Russell, L. M., Jonsson, H. H., and Seinfeld, J. H.: Characterisation and
1515 airborne deployment of a new counterflow virtual impactor inlet, *Atmospheric Measurement*
1516 *Techniques*, 5, 1259–1269, <https://doi.org/10.5194/amt-5-1259-2012>, 2012.
- 1517 Shinozuka, Y., Clarke, A. D., Howell, S. G., Kapustin, V. N., and Huebert, B. J.: Sea-salt vertical
1518 profiles over the Southern and tropical Pacific oceans: Microphysics, optical properties, spatial
1519 variability, and variations with wind speed, *Journal of Geophysical Research: Atmospheres*, 109,
1520 D24201, <https://doi.org/10.1029/2004JD004975>, 2004.
- 1521 Singh, H. B. and Kasting, J. F.: Chlorine-hydrocarbon photochemistry in the marine troposphere
1522 and lower stratosphere, *Journal of Atmospheric Chemistry*, 7, 261–285,
1523 <https://doi.org/10.1007/BF00130933>, 1988.
- 1524 Solomon, S., Stone, K., Yu, P., Murphy, D. M., Kinnison, D., Ravishankara, A. R., and Wang,
1525 P.: Chlorine activation and enhanced ozone depletion induced by wildfire aerosol, *Nature*, 615,
1526 259–264, <https://doi.org/10.1038/s41586-022-05683-0>, 2023.

- 1527 Sorooshian, A., Brechtel, F. J., Ma, Y., Weber, R. J., Corless, A., Flagan, R. C., and Seinfeld, J.
 1528 H.: Modeling and Characterization of a Particle-into-Liquid Sampler (PILS), *Aerosol Science*
 1529 *and Technology*, 40, 396–409, <https://doi.org/10.1080/02786820600632282>, 2006.
- 1530 Sorooshian, A., Murphy, S. M., Hersey, S., Bahreini, R., Jonsson, H., Flagan, R. C., and
 1531 Seinfeld, J. H.: Constraining the contribution of organic acids and AMS m/z 44 to the organic
 1532 aerosol budget: On the importance of meteorology, aerosol hygroscopicity, and region,
 1533 *Geophysical Research Letters*, 37, L21807, <https://doi.org/10.1029/2010GL044951>, 2010.
- 1534 Sorooshian, A., Csavina, J., Shingler, T., Dey, S., Brechtel, F. J., Sáez, A. E., and Betterton, E.
 1535 A.: Hygroscopic and Chemical Properties of Aerosols Collected near a Copper Smelter:
 1536 Implications for Public and Environmental Health, *Environ. Sci. Technol.*, 46, 9473–9480,
 1537 <https://doi.org/10.1021/es302275k>, 2012.
- 1538 Sorooshian, A., Anderson, B., Bauer, S. E., Braun, R. A., Cairns, B., Crosbie, E., Dadashazar,
 1539 H., Diskin, G., Ferrare, R., Flagan, R. C., Hair, J., Hostetler, C., Jonsson, H. H., Kleb, M. M.,
 1540 Liu, H., MacDonald, A. B., McComiskey, A., Moore, R., Painemal, D., Russell, L. M., Seinfeld,
 1541 J. H., Shook, M., Smith, W. L., Thornhill, K., Tselioudis, G., Wang, H., Zeng, X., Zhang, B.,
 1542 Ziemba, L., and Zuidema, P.: Aerosol–Cloud–Meteorology Interaction Airborne Field
 1543 Investigations: Using Lessons Learned from the U.S. West Coast in the Design of ACTIVATE
 1544 off the U.S. East Coast, *Bulletin of the American Meteorological Society*, 100, 1511–1528,
 1545 <https://doi.org/10.1175/BAMS-D-18-0100.1>, 2019.
- 1546 Sorooshian, A., Corral, A. F., Braun, R. A., Cairns, B., Crosbie, E., Ferrare, R., Hair, J., Kleb, M.
 1547 M., Hossein Mardi, A., Maring, H., McComiskey, A., Moore, R., Painemal, D., Scarino, A. J.,
 1548 Schlosser, J., Shingler, T., Shook, M., Wang, H., Zeng, X., Ziemba, L., and Zuidema, P.:
 1549 Atmospheric Research Over the Western North Atlantic Ocean Region and North American East
 1550 Coast: A Review of Past Work and Challenges Ahead, *Journal of Geophysical Research:*
 1551 *Atmospheres*, 125, e2019JD031626, <https://doi.org/10.1029/2019JD031626>, 2020.
- 1552 Sorooshian, A., Alexandrov, M. D., Bell, A. D., Bennett, R., Betito, G., Burton, S. P.,
 1553 Buzanowicz, M. E., Cairns, B., Chemyakin, E. V., Chen, G., Choi, Y., Collister, B. L., Cook, A.
 1554 L., Corral, A. F., Crosbie, E. C., van Dierenhoven, B., DiGangi, J. P., Diskin, G. S., Dmitrovic,
 1555 S., Edwards, E.-L., Fenn, M. A., Ferrare, R. A., van Gilst, D., Hair, J. W., Harper, D. B., Hilario,
 1556 M. R. A., Hostetler, C. A., Jester, N., Jones, M., Kirschler, S., Kleb, M. M., Kusterer, J. M.,
 1557 Leavor, S., Lee, J. W., Liu, H., McCauley, K., Moore, R. H., Nied, J., Notari, A., Nowak, J. B.,
 1558 Painemal, D., Phillips, K. E., Robinson, C. E., Scarino, A. J., Schlosser, J. S., Seaman, S. T.,
 1559 Seethala, C., Shingler, T. J., Shook, M. A., Sinclair, K. A., Smith Jr., W. L., Spangenberg, D. A.,
 1560 Stamnes, S. A., Thornhill, K. L., Voigt, C., Vömel, H., Wasilewski, A. P., Wang, H., Winstead,
 1561 E. L., Zeider, K., Zeng, X., Zhang, B., Ziemba, L. D., and Zuidema, P.: Spatially coordinated
 1562 airborne data and complementary products for aerosol, gas, cloud, and meteorological studies:
 1563 the NASA ACTIVATE dataset, *Earth System Science Data*, 15, 3419–3472,
 1564 <https://doi.org/10.5194/essd-15-3419-2023>, 2023.
- 1565 Su, B., Wang, T., Zhang, G., Liang, Y., Lv, C., Hu, Y., Li, L., Zhou, Z., Wang, X., and Bi, X.: A
 1566 review of atmospheric aging of sea spray aerosols: Potential factors affecting chloride depletion,
 1567 *Atmospheric Environment*, 290, 119365, <https://doi.org/10.1016/j.atmosenv.2022.119365>, 2022.

- 1568 Sullivan, A. P., Guo, H., Schroder, J. C., Campuzano-Jost, P., Jimenez, J. L., Campos, T., Shah,
1569 V., Jaeglé, L., Lee, B. H., Lopez-Hilfiker, F. D., Thornton, J. A., Brown, S. S., and Weber, R. J.:
1570 Biomass Burning Markers and Residential Burning in the WINTER Aircraft Campaign, *Journal*
1571 *of Geophysical Research: Atmospheres*, 124, 1846–1861,
1572 <https://doi.org/10.1029/2017JD028153>, 2019.
- 1573 Sullivan, R. C., Guazzotti, S. A., Sodeman, D. A., and Prather, K. A.: Direct observations of the
1574 atmospheric processing of Asian mineral dust, *Atmospheric Chemistry and Physics*, 7, 1213–
1575 1236, <https://doi.org/10.5194/acp-7-1213-2007>, 2007.
- 1576 Takegawa, N., Miyakawa, T., Kawamura, K., and Kondo, Y.: Contribution of Selected
1577 Dicarboxylic and ω -Oxocarboxylic Acids in Ambient Aerosol to the m/z 44 Signal of an
1578 Aerodyne Aerosol Mass Spectrometer, *Aerosol Science and Technology*, 41, 418–437,
1579 <https://doi.org/10.1080/02786820701203215>, 2007.
- 1580 Tanaka, P. L., Riemer, D. D., Chang, S., Yarwood, G., McDonald-Buller, E. C., Apel, E. C.,
1581 Orlando, J. J., Silva, P. J., Jimenez, J. L., Canagaratna, M. R., Neece, J. D., Mullins, C. B., and
1582 Allen, D. T.: Direct evidence for chlorine-enhanced urban ozone formation in Houston, Texas,
1583 *Atmospheric Environment*, 37, 1393–1400, [https://doi.org/10.1016/S1352-2310\(02\)01007-5](https://doi.org/10.1016/S1352-2310(02)01007-5),
1584 2003.
- 1585 Tang, I. N., Tridico, A. C., and Fung, K. H.: Thermodynamic and optical properties of sea salt
1586 aerosols, *Journal of Geophysical Research: Atmospheres*, 102, 23269–23275,
1587 <https://doi.org/10.1029/97JD01806>, 1997.
- 1588 Tang, M., Guo, L., Bai, Y., Huang, R.-J., Wu, Z., Wang, Z., Zhang, G., Ding, X., Hu, M., and
1589 Wang, X.: Impacts of methanesulfonate on the cloud condensation nucleation activity of sea salt
1590 aerosol, *Atmospheric Environment*, 201, 13–17, <https://doi.org/10.1016/j.atmosenv.2018.12.034>,
1591 2019.
- 1592 Thornhill, K. L., Anderson, B. E., Barrick, J. D. W., Bagwell, D. R., Friesen, R., and Lenschow,
1593 D. H.: Air motion intercomparison flights during Transport and Chemical Evolution in the
1594 Pacific (TRACE-P)/ACE-ASIA, *Journal of Geophysical Research: Atmospheres*, 108, 8783,
1595 <https://doi.org/10.1029/2002JD003108>, 2003.
- 1596 Thornton, J. A., Kercher, J. P., Riedel, T. P., Wagner, N. L., Cozic, J., Holloway, J. S., Dubé, W.
1597 P., Wolfe, G. M., Quinn, P. K., Middlebrook, A. M., Alexander, B., and Brown, S. S.: A large
1598 atomic chlorine source inferred from mid-continental reactive nitrogen chemistry, *Nature*, 464,
1599 271–274, <https://doi.org/10.1038/nature08905>, 2010.
- 1600 Toole, D. A. and Siegel, D. A.: Light-driven cycling of dimethylsulfide (DMS) in the Sargasso
1601 Sea: Closing the loop, *Geophysical Research Letters*, 31, L09308,
1602 <https://doi.org/10.1029/2004GL019581>, 2004.
- 1603 Ullerstam, M., Vogt, R., Langer, S., and Ljungström, E.: The kinetics and mechanism of SO₂
1604 oxidation by O₃ on mineral dust, *Phys. Chem. Chem. Phys.*, 4, 4694–4699,
1605 <https://doi.org/10.1039/B203529B>, 2002.

- 1606 Vallina, S. M. and Simó, R.: Strong Relationship Between DMS and the Solar Radiation Dose
1607 over the Global Surface Ocean, *Science*, 315, 506–508, <https://doi.org/10.1126/science.1133680>,
1608 2007.
- 1609 Van Rooy, P., Drover, R., Cress, T., Michael, C., Purvis-Roberts, K. L., Silva, P. J., Nee, M. J.,
1610 and Cocker, D.: Methanesulfonic acid and sulfuric acid Aerosol Formed through oxidation of
1611 reduced sulfur compounds in a humid environment, *Atmospheric Environment*, 261, 118504,
1612 <https://doi.org/10.1016/j.atmosenv.2021.118504>, 2021.
- 1613 Wang, X., Jacob, D. J., Downs, W., Zhai, S., Zhu, L., Shah, V., Holmes, C. D., Sherwen, T.,
1614 Alexander, B., Evans, M. J., Eastham, S. D., Neuman, J. A., Veres, P. R., Koenig, T. K.,
1615 Volkamer, R., Huey, L. G., Bannan, T. J., Percival, C. J., Lee, B. H., and Thornton, J. A.: Global
1616 tropospheric halogen (Cl, Br, I) chemistry and its impact on oxidants, *Atmospheric Chemistry
1617 and Physics*, 21, 13973–13996, <https://doi.org/10.5194/acp-21-13973-2021>, 2021.
- 1618 Wittig, V. E., Ainsworth, E. A., Naidu, S. L., Karnosky, D. F., and Long, S. P.: Quantifying the
1619 impact of current and future tropospheric ozone on tree biomass, growth, physiology and
1620 biochemistry: a quantitative meta-analysis, *Global Change Biology*, 15, 396–424,
1621 <https://doi.org/10.1111/j.1365-2486.2008.01774.x>, 2009.
- 1622 Wu, Y., Han, Z., Nazmi, C., Gross, B., and Moshary, F.: A trans-Pacific Asian dust episode and
1623 its impacts to air quality in the east coast of U.S., *Atmospheric Environment*, 106, 358–368,
1624 <https://doi.org/10.1016/j.atmosenv.2015.02.013>, 2015.
- 1625 Yan, J., Jung, J., Zhang, M., Bianchi, F., Tham, Y. J., Xu, S., Lin, Q., Zhao, S., Li, L., and Chen,
1626 L.: Uptake selectivity of methanesulfonic acid (MSA) on fine particles over polynya regions of
1627 the Ross Sea, Antarctica, *Atmospheric Chemistry and Physics*, 20, 3259–3271,
1628 <https://doi.org/10.5194/acp-20-3259-2020>, 2020.
- 1629 Yao, X. and Zhang, L.: Chemical processes in sea-salt chloride depletion observed at a Canadian
1630 rural coastal site, *Atmospheric Environment*, 46, 189–194,
1631 <https://doi.org/10.1016/j.atmosenv.2011.09.081>, 2012.
- 1632 Yokelson, R. J., Crouse, J. D., DeCarlo, P. F., Karl, T., Urbanski, S., Atlas, E., Campos, T.,
1633 Shinozuka, Y., Kapustin, V., Clarke, A. D., Weinheimer, A., Knapp, D. J., Montzka, D. D.,
1634 Holloway, J., Weibring, P., Flocke, F., Zheng, W., Toohey, D., Wennberg, P. O., Wiedinmyer,
1635 C., Mauldin, L., Fried, A., Richter, D., Walega, J., Jimenez, J. L., Adachi, K., Buseck, P. R.,
1636 Hall, S. R., and Shetter, R.: Emissions from biomass burning in the Yucatan, *Atmospheric
1637 Chemistry and Physics*, 9, 5785–5812, <https://doi.org/10.5194/acp-9-5785-2009>, 2009.
- 1638 Young, A. H., Keene, W. C., Pszenny, A. A. P., Sander, R., Thornton, J. A., Riedel, T. P., and
1639 Maben, J. R.: Phase partitioning of soluble trace gases with size-resolved aerosols in near-surface
1640 continental air over northern Colorado, USA, during winter, *Journal of Geophysical Research:
1641 Atmospheres*, 118, 9414–9427, <https://doi.org/10.1002/jgrd.50655>, 2013.
- 1642 Young, C. J., Washenfelder, R. A., Edwards, P. M., Parrish, D. D., Gilman, J. B., Kuster, W. C.,
1643 Mielke, L. H., Osthoff, H. D., Tsai, C., Pikelnaya, O., Stutz, J., Veres, P. R., Roberts, J. M.,
1644 Griffith, S., Dusanter, S., Stevens, P. S., Flynn, J., Grossberg, N., Lefer, B., Holloway, J. S.,

- 1645 Peischl, J., Ryerson, T. B., Atlas, E. L., Blake, D. R., and Brown, S. S.: Chlorine as a primary
1646 radical: evaluation of methods to understand its role in initiation of oxidative cycles,
1647 Atmospheric Chemistry and Physics, 14, 3427–3440, <https://doi.org/10.5194/acp-14-3427-2014>,
1648 2014.
- 1649 Zhang, D. and Iwasaka, Y.: Chlorine deposition on dust particles in marine atmosphere,
1650 Geophysical Research Letters, 28, 3613–3616, <https://doi.org/10.1029/2001GL013333>, 2001.
- 1651 Zhang, Q., Alfarra, M. R., Worsnop, D. R., Allan, J. D., Coe, H., Canagaratna, M. R., and
1652 Jimenez, J. L.: Deconvolution and Quantification of Hydrocarbon-like and Oxygenated Organic
1653 Aerosols Based on Aerosol Mass Spectrometry, Environ. Sci. Technol., 39, 4938–4952,
1654 <https://doi.org/10.1021/es048568l>, 2005.
- 1655 Zhao, Y. and Gao, Y.: Acidic species and chloride depletion in coarse aerosol particles in the US
1656 east coast, Science of The Total Environment, 407, 541–547,
1657 <https://doi.org/10.1016/j.scitotenv.2008.09.002>, 2008.
- 1658 Ziemba, L. D., Griffin, R. J., Whitlow, S., and Talbot, R. W.: Characterization of water-soluble
1659 organic aerosol in coastal New England: Implications of variations in size distribution,
1660 Atmospheric Environment, 45, 7319–7329, <https://doi.org/10.1016/j.atmosenv.2011.08.022>,
1661 2011.
- 1662 Zorn, S. R., Drewnick, F., Schott, M., Hoffmann, T., and Borrmann, S.: Characterization of the
1663 South Atlantic marine boundary layer aerosol using an aerodyne aerosol mass spectrometer,
1664 Atmospheric Chemistry and Physics, 8, 4711–4728, <https://doi.org/10.5194/acp-8-4711-2008>,
1665 2008.
- 1666 Zuidema, P., Alvarez, C., Kramer, S. J., Custals, L., Izaguirre, M., Sealy, P., Prospero, J. M., and
1667 Blades, E.: Is Summer African Dust Arriving Earlier to Barbados? The Updated Long-Term In
1668 Situ Dust Mass Concentration Time Series from Ragged Point, Barbados, and Miami, Florida,
1669 Bulletin of the American Meteorological Society, 100, 1981–1986,
1670 <https://doi.org/10.1175/BAMS-D-18-0083.1>, 2019.

1671